April 2012

Self-balancing in Rotating Machinery

Cody Joseph Harrop
Worcester Polytechnic Institute

Eric Charles Montague
Worcester Polytechnic Institute

Vu Dang Nguyen
Worcester Polytechnic Institute

Final Report

as a partial requirement for

Major Qualifying Project

Self-balancing in Rotating Machinery

Submitted by:

_____
Cody Harrop

_____
Eric Montague

_____
Vu Nguyen

Submitted to:

Professor Mikhail Dimentberg
Professor John Hall

Mechanical Engineering Department
Worcester Polytechnic Institute
Worcester, MA 01609-2280

April 26, 2012

Acknowledgement

We would like to express our special thank Professor Mikhail F. Dimentberg and Professor John R. Hall for offering us an opportunity to work on this exciting project and providing many valuable advices. We also want to thank Professor Ryszard J. Pryputniewicz who gives us access to the equipment in Center for Holographic Studies and Laser μmechaTronics (CHLST) and Mr. Peter Hefti who offers us generous help with our stroboscopic experiments. Also thanks to lab specialists in Washburn manufacturing lab who also offer us great help during the fabrication of our devices.

Contents

List of Figures

List of Tables

Abstract

In rotating machinery, mass imbalances are unavoidable and can lead to large vibrating forces and displacements. These imbalances, which in many cases are unknown, can be corrected by a passive balancing system, which is more advantageous than an active balancing system in terms of complexity, as it does not require a sensor-actuator system. The project will investigate the method of passively correcting mass imbalances in a rotor operating above its critical speed using ball balancers. This passive balancing phenomenon will be described theoretically and a working model will be fabricated to demonstrate this principle. The device will also be used to test the ability of the ball balancers to achieve a stable balancing position under different conditions including rotation speed, number of ball balancers, addition of damping fluid, and critical speed of the system. Ball positions will be observed with stroboscopic illumination and the vibration of the rotor will be measured using two piezoelectric accelerometers.

I. Introduction

Rotating machinery is widely used in a variety of applications such as aerospace, energy, machining equipment, or even household equipment such as washing machine or CD player. One major problem in these devices is the vibration caused by its unbalanced mass, which happens when the center of mass does not coincide with the axis of rotation. Moreover, this unbalanced mass is not necessarily constant but can also vary with time or unknown, as we can clearly observe, for example, in the washing machine. Thus there is a need to have a mechanism to conveniently balance out the varying unbalanced mass. An active balancer, in which an added mass will be actuated by a control system to move to the balancing position, can add much complexity, cost and weight to the original device. In this project, we will attempt to build and test a passive balancer that can also achieve self-balancing like the active balancer but in a much simpler and less expensive way. This passive balancer eliminates the need of sensor, actuator and control system by taking advantage of a physical phenomenon occurring when the machine is rotating at a speed above its critical speed. This phenomenon will automatically move an added mass to a position that cancels the eccentric mass of the machine. The passive balancer we will investigate is a ball balancer, in which some number of balls is added into the machine and they can freely move into balancing positions. This project will aim to design, analyze, build and test this ball balancer.

II. Background

II.1. Literature review

First, the self-balancing phenomenon using balls can be explained by Figure 1. In case of no damping and the rotating speed of the disk is below resonant frequency, the geometric center C will rotate in phase with the centrifugal force, so the phase angle is zero and G is outside OC. Such situation is not of our interest. However, in case of no damping, when the rotating speed of the disk is above resonant frequency, the vibration of the geometric center C will be 180 degree out of phase with the centrifugal force, so the mass center G will always be inside OC. This phenomenon is demonstrated by the plot in Figure 7 in section II.2. We are interested in this situation because it is possible for self-balancing to occur. If G is always inside OC and we have masses, such as balls, that can freely move within the disk, the centrifugal force from the rotation of C around O will keep the freely moving masses in the opposite side of G with respect to C and balance the eccentric mass. In reality there will be damping and the phase angle will be smaller than 180 degree at a practical rotational speed.

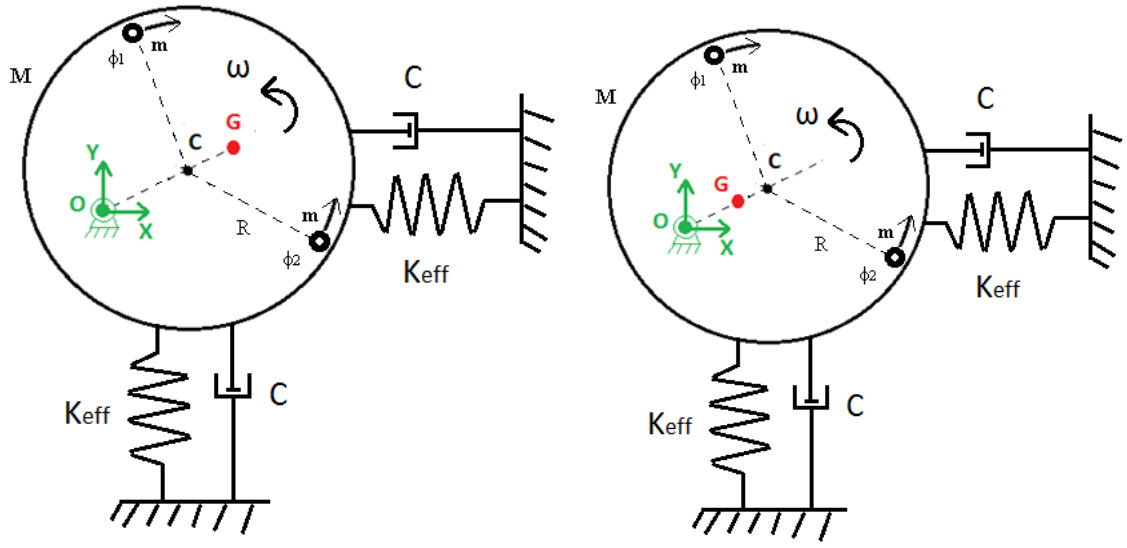

Figure 1. Schematic of the model for the eccentric disk with ball balancer. Rotation speed is pre-resonant in the left image and post-resonant in the right image.

The phenomenon of passive self-balancing has been studied by many researchers. The ball balancer was analytically studied by Blekhman. He showed the equations of motion for the rotor with n-ball balancer and proved that for the case n=2 the steady-state positions of the balls in post-resonance speed are stable. (Blekhman, 1988).

In other papers, Green et al. (2008) and Chung et al. (2003) also obtain the same equations of motion, despite in different form, using Lagrange approach. Green et al. have put the equations of motion into dimensionless matrix form:

$$\begin{pmatrix} 1+n\mu & 0 \\ 0 & 1+n\mu \end{pmatrix}\begin{pmatrix} \ddot{x} \\ \ddot{y} \end{pmatrix} + \begin{pmatrix} 2\zeta & -2\Omega(1+n\mu) \\ 2\Omega(1+n\mu) & 2\zeta \end{pmatrix}\begin{pmatrix} \dot{x} \\ \dot{y} \end{pmatrix} + \begin{pmatrix} K & -2\Omega\zeta \\ 2\Omega\zeta & K \end{pmatrix}\begin{pmatrix} x \\ y \end{pmatrix} = \begin{pmatrix} \delta\Omega^2 \\ 0 \end{pmatrix} + \mu\sum_{i=1}^{n}\begin{pmatrix} (\Omega+\dot{\phi}_\iota)^2 & \ddot{\phi}_\iota \\ -\ddot{\phi}_\iota & (\Omega+\dot{\phi}_\iota)^2 \end{pmatrix}\begin{pmatrix} cos\phi_i \\ sin\phi_i \end{pmatrix} \quad (1)$$

and the motion of the *i*th ball is:

$$\ddot{\phi}_\iota + \beta\dot{\phi}_\iota - (\ddot{x} - \Omega^2 x - 2\Omega\dot{y})sin\phi_i + (\ddot{y} - \Omega^2 y + 2\Omega\dot{x})cos\phi_i = 0 \quad (2)$$

where x and y are coordinates of the center of the disk C in the rotating frame xOy. Ω, ζ, β, μ, δ are dimensionless parameters defined as:

$$\Omega = \frac{\omega}{\omega_n},\ \ \zeta = \frac{C}{2\sqrt{K_{eff}M}},\ \ \beta = \frac{D}{mR^2\omega_n},\ \ \mu = \frac{m}{M},\ \ \delta = \frac{\varepsilon}{R},$$

where ω and ω_n are rotational speed and resonant frequency of the system respectively, and ε is the distance CG, M is the mass of the disk and m is the mass of each ball. All the parameters of this model are shown in Figure 1.

Due to time limitation, we were not able to numerically simulate equation (1) and (2) with our own parameters. On the other hand, Green et al. have numerically solved those

equations for the decaying absolute magnitude of vibration $r = \sqrt{x^2 + y^2}$ with his model, which is shown in Figure 2.

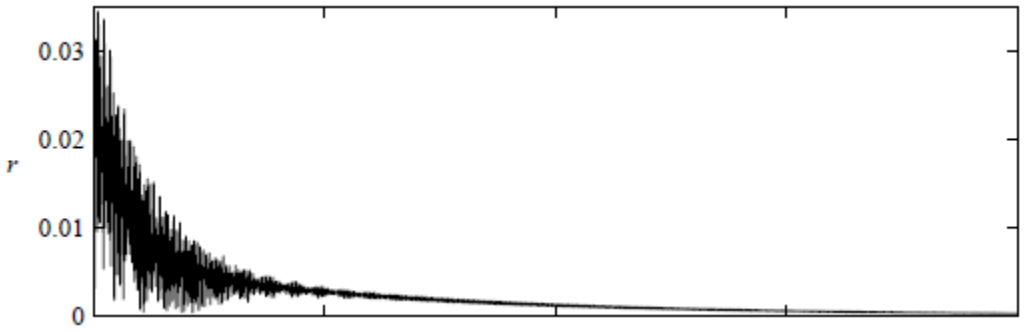

Figure 2. Absolute magnitude of vibration vs. time for 2-ball balancer (Green, 2008).

Also, Green et al. argued that there is no general conclusion on the optimal number of balls, and it should depend on the specific implementation of the ball balancer.

Chung et al. have also investigated the equation (1) and (2) to analyze the stability of the equilibrium state by applying Routh-Hurwitz criterion for negative real part of the eigenvalue. One of his conclusions is that the damping D of the balls' movement in the groove plays a crucial role, as the balancing of the eccentric rotor cannot be achieved at D=0. Damping of the translational motion of the disk is also required, according to Chung et al.

Another interesting work is by Horvath et al. (Horvath, 2008), who analyzed and tested two types of passive balancers: ball and pendulum balancers. The pendulum balancer is basically the same idea as the ball balancer: instead of the balls being guided in a groove, they are now attached to the center by a rigid bar to become a pendulum. The balls of the pendulum find their balancing positions the same way as the balls in a groove. Although Horvath's work mainly focused on pendulum balancers, he also presented results for his experiment with 2-ball balancers, shown in Figure 3.

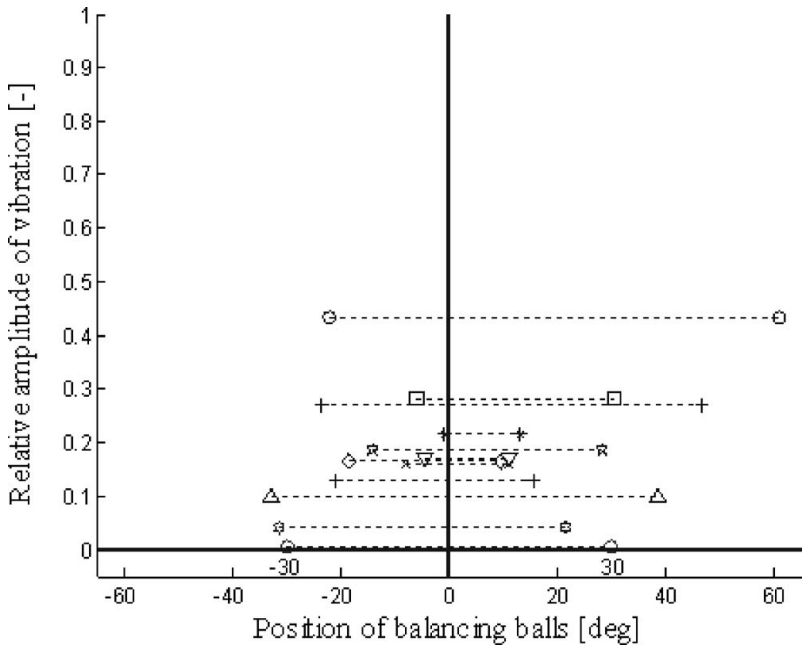

Figure 3. Final positions of balancing balls and the level of vibration for different startups (Horvath, 2008).

Figure 3 shows the settled positions of the balls under different startups, in each of which the motor is turned off until stop and turned on again up to 1500 rpm. Ideal positions of the two balls are at -30 and 30 degree. As the test is repeated a number of times, the two balls end up in a variety of positions, some are very close to the ideal positions, some are very off. However, for all tests a reduction in the vibration amplitude was always recorded. Horvath attributed the low repeatability of the tests to the deformation of the contact point between the ball and the groove surface of the disk due to high centrifugal force.

II.2. Theoretical analysis

To perform theoretical analysis, we first consider two shaft configurations: horizontal shaft and vertical shaft. The dynamic models for the two configurations are shown in Figure 4

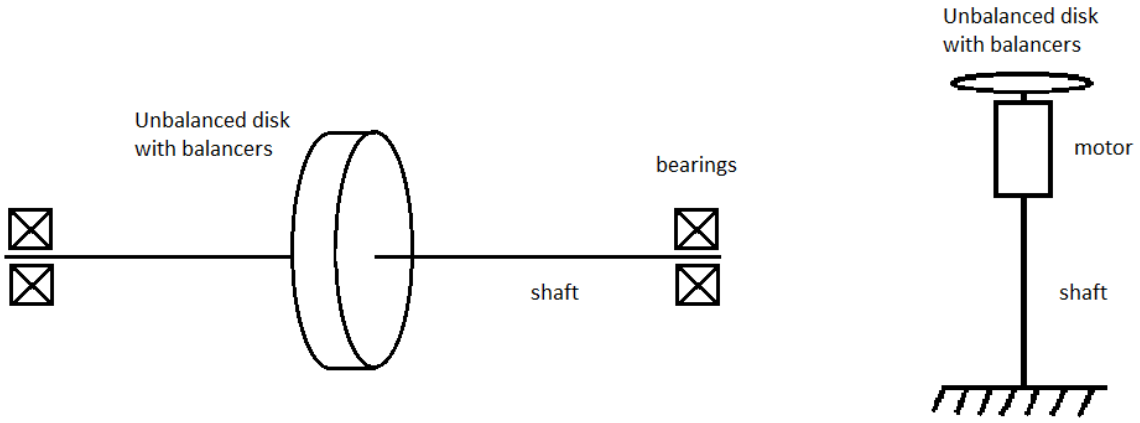

Figure 4. Horizontal and vertical shaft configurations.

Resonant frequency for each configuration is estimated to decide which configuration we should pursue to create. In this project, we are only interested in the first resonant frequency, since higher resonant frequencies would not affect the stability of the balls' positions. For safety issue, we want to limit the motor speed to about 1000-1500rpm and use a steel shaft. The bearing fixture can allow some whirling of the shaft, so it can be considered a type of fixture between clamp and pin. Thus the first resonant frequency for the horizontal shaft with two bearing fixture at the two ends can be estimated by equation:

$$\frac{1}{2\pi}\sqrt{\frac{48EI}{L^3(M+0.5m_{shaft})}} < f_n < \frac{1}{2\pi}\sqrt{\frac{192EI}{L^3(M+0.5m_{shaft})}} \quad (3)$$

where E is Young modulus of steel, I is the second moment of area of the shaft cross-section, L is the total length of the shaft, and M is the mass at the middle of the shaft. 48 is the coefficient for pin-pin fixture, and 192 is the coefficient for clamp-clamp fixture. The value for natural frequency will be given as the above range.

For vertical shaft, we can mount the motor on one end and eliminate the need of bearings. Thus first resonant frequency for the vertical shaft can be estimated by the equation for clamp-clamp beam:

$$f_n = \frac{1}{2\pi}\sqrt{\frac{3EI}{L^3(M + 0.23m_{shaft})}} \quad (4)$$

where L is the distance from the fixture to the center of mass at the top, and M is the effective mass at the top.

From our preliminary model, we iterated several calculations to estimate resonant frequencies and summarize it in Table 1.

Table 1. Iterations to estimate resonant frequency for the two configurations.

	Horizontal configuration			**Vertical configuration**		
Effective mass	2.6kg	2.3kg	2.4kg	4.9kg	4.7kg	4.8kg
Effective length	400mm	400mm	600mm	400mm	400mm	600mm
Shaft diameter	20mm	12mm	12mm	20mm	12mm	12mm
Resonant frequency	6400rpm-12,870rpm	2500rpm-4900rpm	1300rpm-2600rpm	1200rpm	430rpm	230rpm

Table 1 shows that for the horizontal configuration with two fixtures, to bring the resonant frequency down to the capability of our selected motor, the shaft needs to be much longer and thinner than those in the vertical configuration. Also in this design the shaft would rotate and be driven by a shaft coupling, belt, or chain at one end. In our analysis of the horizontal design, there are two major problems. The balls and disk are subject to the effects of gravity and may have an unusual or even unpredictable behavior. This horizontal configuration

also had the potential to introduce extra noise into our experimental data. The power transmission device(s) required to couple the motor to the shaft and handle any potential misalignment are sources of vibration that do not directly relate to our study of the self-balancing mechanism. This extra vibration would introduce an unnecessary additional variable to the experiment. Our idea for solving the gravity issue was to take the same configuration and mount the shaft vertically, so the disk was aligned in a horizontal plane. However with two fixtures to support the beam it would require a significant structure to make the support points stable and rigid enough to model the shaft and disk as the vibrating system and ignore the flexibility of the support. Also it had no effect on the potential vibration source of the power transmission path. Thus we decided to pursue the clamped-free vertical configuration in which the motor is mounted directly on top of the vertical shaft.

Account for gyroscopic effect.

In the vertical configuration, the natural frequency estimated in equation (4) is not entirely accurate because the gyroscopic effect has not been taken into account. This effect happens due to the fact that there needs to be a torque to change the angular momentum of a rotating part, or in other words, the rotating disk in our case will tend to resist the tilt of its rotation axis caused by the bending of the shaft. Thus the vibration amplitude will be smaller and the shaft seems to be stiffer, which will cause an increase in the natural frequency. Therefore the purpose of this part is to investigate how much the gyroscopic effect will shift the natural frequency in our case. Hartog (1985) derives the expression to account for this shift in natural frequency. He introduces the dimensionless form of the natural frequency:

$$K = (2\pi f_n)\sqrt{\frac{ml^3}{EI}} \tag{5}$$

The dimensionless natural frequency with the gyroscopic effect is then:

$$K^2 = \left(6 - \frac{2}{D}\right) + \sqrt{\left(6 - \frac{2}{D}\right)^2 + \frac{12}{D}} \tag{6}$$

where

$$D = \frac{I_d}{ml^2}$$

where I_d is the moment of inertia of the disk along one of its diameter, which is (1/4)(mR^2), m is the mass of the disk, and l is the length of the shaft. To calculate the gyroscopic effect for our model, we will assume that all the effective mass on top of the shaft will be distributed evenly in the rotating disk so that the gyroscopic effect will be maximized. The new frequency calculated is:

$$f_{n\_gyro} = \frac{K}{2\pi}\sqrt{\frac{EI}{ml^3}} \approx 14.15Hz \tag{7}$$

Without the gyroscopic, the natural frequency is about 13.92Hz. Thus, although the natural frequency is increased as expected, it increases only less than 2%. As a result, the gyroscopic effect will be neglected in our future analysis.

Estimated unbalanced vibration

The vibration of the unbalanced disk without the balancers for the vertical shaft configuration is analyzed in this section. The schematic of the rotating unbalanced disk from the top view can be found in Figure 1 Section II.1. O is the fixture, C is the geometric center of the disk where the shaft is attached, G is the offset center of mass of the disk, and φ is the phase angle between OC and CG. The position of the geometric center C can be represented by a complex number Z (Dimentberg, 2010):

$$Z_C = X_C + iY_C \tag{8}$$

If there is no unbalance, C will locate at O, Z_C is always zero and there is no vibration. Practically there will be unbalance and the centrifugal force will pull C away from O. Let $Z_C = Z_0 \exp(i2\pi ft)$, the steady-state solution for Z_0 is given by the equation (Dimentberg, 2010):

$$Z_0 = \frac{M_{eff}(2\pi f)^2 e_G}{K_{eff} - M_{eff}(2\pi f)^2 + i(2\pi f)c_d} \tag{9}$$

where M_{eff} and K_{eff} are effective mass and effective stiffness of the shaft respectively, f is the rotational frequency of the disk in Hz, c_d is the external damping coefficient, which is caused by fixture, and e_G is distance between C and G.

The amplitude of the vibration of the geometric center C is the magnitude of the complex number Z_0:

$$A_C = |Z_0| \tag{10}$$

The phase angle between OC and CG is:

$$\varphi = \arctan\left[\frac{Im(Z_0)}{Re(Z_0)}\right] \tag{11}$$

We will calculate the theoretical response of the unbalanced disk without the balancers based on dimensions and masses obtained from our CAD model. Theoretical calculation and CAD model are iterated several times to give us a range of data before we fabricate the mechanism. To estimate the damping coefficient, which we do not know from our CAD model, we estimate that in an impact test, the signal of the vibration is still observable within 5s. Using

the calculated natural frequency of the system, we are able to plot some damped responses for different damping coefficients, represented by the percentage of critical damp. From Figure 5, we figure out that 0.5% to 5% of critical damp is reasonable range for damping coefficient.

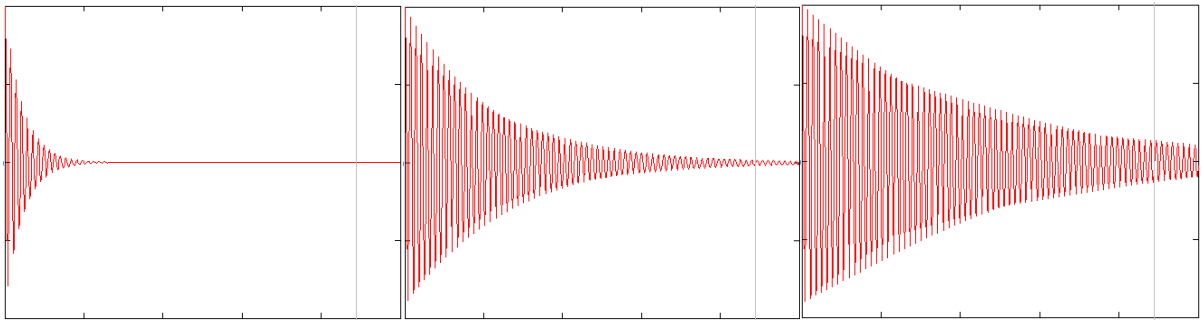

Figure 5. Response within 5s for, from left to right, 5%, 1% and 0.5% of critical damp.

Based on the analysis in previous section, we find the dimensions and effective mass of the system that give a reasonable resonant frequency and plot the responses for different damping coefficient. The values used in our theoretical model are summarized in Table 2.

Table 2. Values used in theoretical model.

Quantity	**Value**
Shaft length	500mm
Shaft diameter	20mm
Young modulus of steel	200GPa
Effective mass (disk, unbalance, motor, mounting components and $0.23m_{shaft}$)	4.9kg
Unbalance mass	0.1kg
Distance from the unbalance to the disk's center	10mm-50mm
Damping coefficient as a percentage of critical damp	0.5%-5%

Figure 6 and 7 are plot of the disk's vibration amplitude and the phase angle of the center of mass G of the disk.

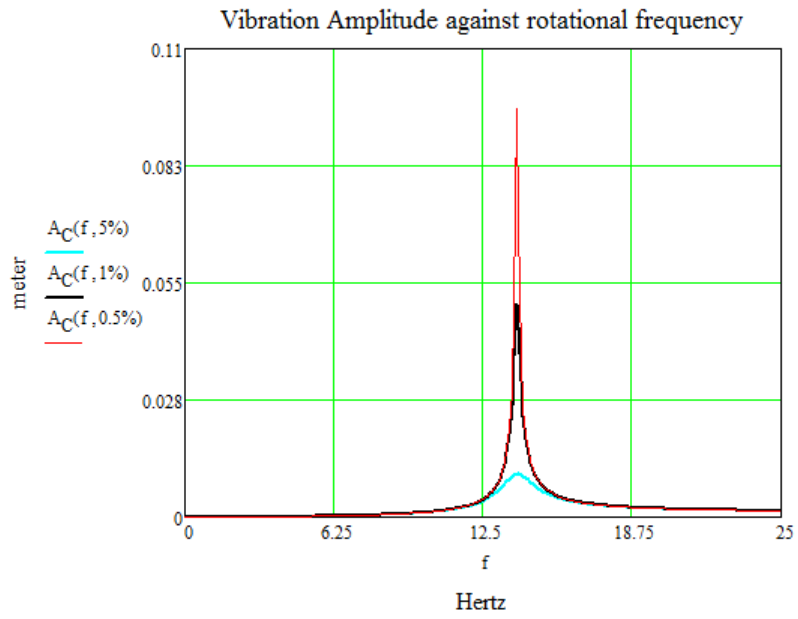

Figure 6. Vibration amplitude versus rotational speed. The peak is at resonant frequency.

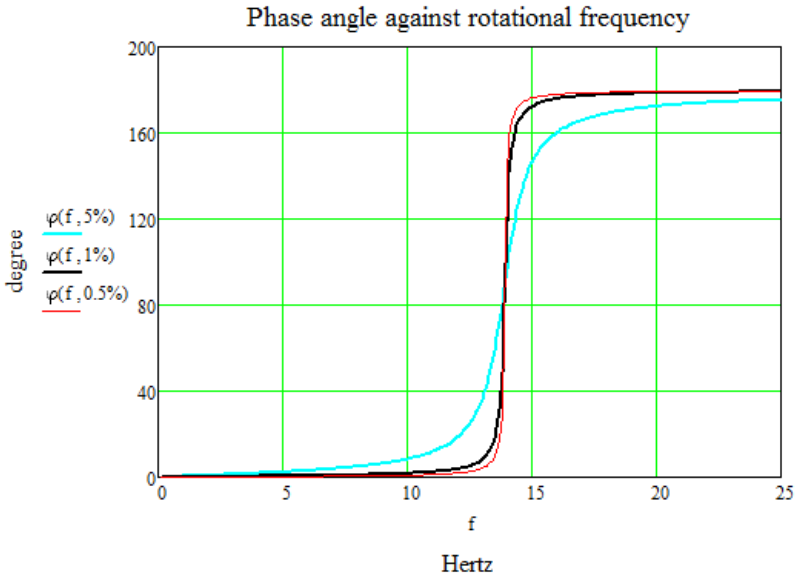

Figure 7. Phase angle versus rotational frequency. 90 degree is at resonant frequency.

In order for the self-balancing to happen, the motor needs to run at speed above resonant frequency. Thus, we calculate the response of the disk at 1.5 resonant frequency and summarize the results in Table 3.

Table 3. Summary of the response for our theoretical model.

Dynamic length (mm)	Shaft diameter (mm)	Natural frequency (Hz)	Unbalance position and Eccentricity (mm)	Percent of critical damp (%)	Amplitude at f=1.5fn (mm)	Phase at f=1.5fn (deg)
500	20	13.9	50 (1.02)	5	1.8	173
				1	1.8	179
				0.5	1.8	179
			30 (0.609)	5	1.1	173
				1	1.1	179
				0.5	1.1	179
			10 (0.203)	5	0.4	173
				1	0.4	179
				0.5	0.4	179

It is shown that the phase angle is nearly 180 degree. Vibration amplitude of 1 to 2 mm is detectable. The last note of this section is that, to balance the eccentricity listed in Table 3, the number of balls n needs to satisfy the equation:

$$nm_{ball}R_{ball} > M_{eff}\varepsilon \approx m_{unbal}d_{unbal} \quad (12)$$

The approximation in equation (12) occurs when the eccentricity of the disk itself without unbalance is negligible.

Static and Dynamic Analysis

A preliminary static and dynamic loading analysis is done to check if our device can sustain the vibration during tests or will yield or fatigue. There are many parts but we will analyze the shaft since it endures the highest force. This analysis is done at the planned operating speed of 1.5 times the resonant frequency. The model used for this analysis is a cantilever beam shown in Figure 8.

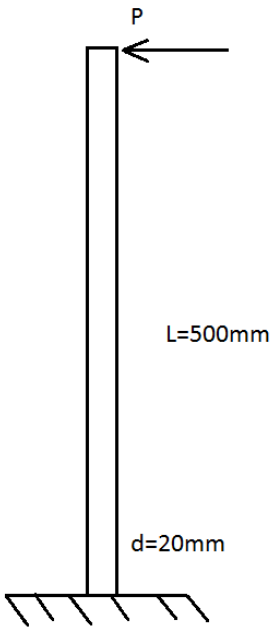

Figure 8. Cantilever model with a point load P.

The force P is caused by the rotating eccentric disk. We calculated in Table 3 that at our operating speed $1.5f_n$ and the unbalance position of 50mm, the amplitude of vibration is 1.8mm. Thus, the applied force can be calculated by multiplying the beam stiffness by that displacement.

$$\mathrm{P} = K_{eff}A \approx 69N \tag{13}$$

The location on the shaft that encounters the greatest stress is on the surface of the shaft at the fixture. The normal stress at that location is calculated by the equation:

$$\sigma = \frac{PLr_{shaft}}{I_{shaft}} \approx 44MPa \tag{14}$$

Since there is only normal stress at this location, the equivalent Von-Mises stress is also the same as the normal stress. The yield strength of AISI 1020 is Y=351.57MPa as provided in the CAD software. Thus the static safety factor is

$$N_{static} = \frac{Y}{\sigma} = 8 \tag{15}$$

There is no stress concentration because the geometry of the shaft does not change from the fixture to the mass at the top.

To analyze fatigue strength, we use criteria described in Norton (2011). First, we need to determine the mean and alternating stress. From static analysis, the mean and alternating stresses are:

$$\sigma_m = 0 \quad \sigma_a = 44MPa \tag{16}$$

Endurance limit S_e for the steel in our model is:

$$S'_e \cong 0.5S_{UTS} = 210.5MPa \tag{17}$$

To determine the fatigue strength as a criterion for fatigue failure, correction factors needs to be applied on the endurance limit. Summary of the correction factors are in Table 4.

Table 4. Fatigue strength correction factors. See Appendix for Mathcad calculation.

Factor	Type	Value
Loading effect	Bending	C_{load}=1
Size effect	8mm<d<250mm	C_{size}=0.889
Surface effect	Cold-rolled	$C_{surface}$=0.909
Temperature	<450^{o}C	C_{temp}=1
Reliability	95%	C_{reli}=0.868

Therefore:

$$S_e = C_{load}C_{size}C_{surf}C_{temp}C_{reli}S'_e \approx 148MPa \tag{18}$$

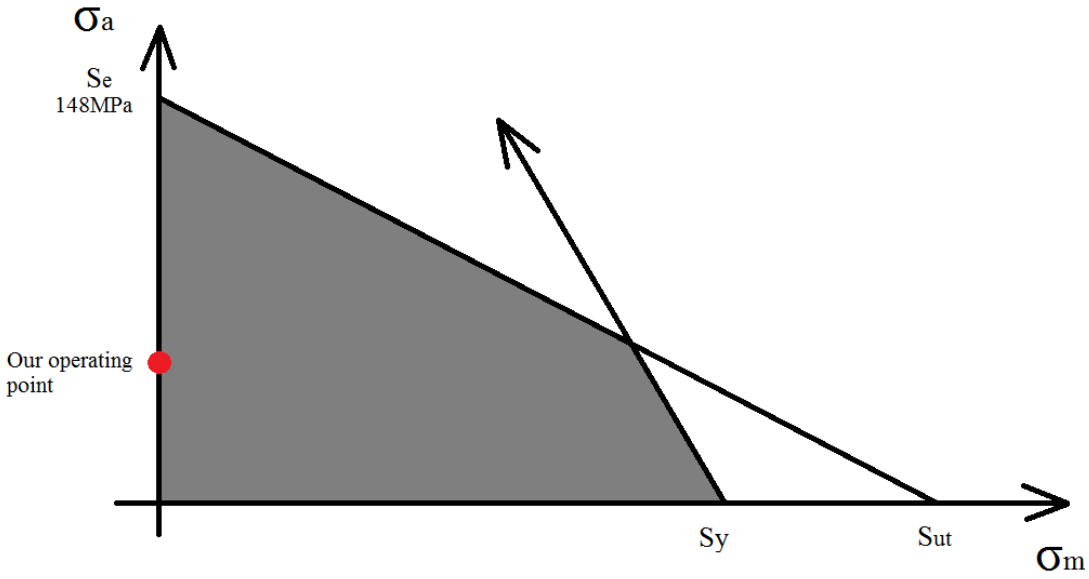

Figure 9. Modified Goodman diagram. Safe region is shaded (Sy is yield strength).

Thus our safety factor for fatigue failure is:

$$N_{dynamic} = \frac{S_e S_{UTS}}{\sigma_a S_{UTS} + \sigma_m S_e} = \frac{S_e}{\sigma_a} = 3.4 \tag{19}$$

This safety factor means that under the specified dynamic load, the life cycle of the shaft is infinity (larger 10^8 cycles). Figure 9 show a modified Goodman diagram of mean stress and alternating stress with our operating point.

III. Design and Fabrication

Our final design was inspired by the design of a prototype mechanism used in a paper we read as background to the self-balancing concept (Horvath, 2008). The inspirational design uses a non-rotating vertical shaft with a motor mounted at the end with the spinning disk affixed directly to the motor shaft. Their design allows the vertical shaft to pivot at the bottom where it meets the base, and relies on springs farther up the shaft near the disk to supply the stiffness of the system. Our design uses a similar non-rotating vertical shaft with the motor and disk mounted to the end, but we chose to control the stiffness and vibration differently. Instead of supporting the top of the shaft with springs we chose to set up the system as a vertical cantilever beam with a clamped support at the base and the top free to move.

III.1. Motor and Motor Controller Selection

Once the basic configuration of a non-rotating vertical clamped cantilever was selected, detailed design down to the individual components began. The primary design consideration for this device is resonant frequency since the balancing mechanism does not function below resonance. In our analysis the motor had the biggest effect on the resonant frequency. The motor is only one variable in calculating the resonant frequency of the system, but the choice of motor dictated our resonant frequency because we needed to be able to comfortably achieve speeds above resonance. In order to easily achieve speeds past the resonant frequency we wanted the first order resonant frequency to occur at less than half the top speed of our motor. To keep the device relatively safe we also wanted to keep the top speed around 2000-3000 rpm in order to stay far away from the possibility of a flywheel explosion caused by exceeding the strength of the metal flywheel.

In order to observe the effects of speed on the balancing mechanism we wanted to be able to vary the motor speed. We explored multiple potential methods for a variable speed motor.

Using an AC motor and variable frequency drive was rejected because of cost. A DC stepper motor was rejected because of the complexity of the control system and the low torque. A DC servomotor was rejected because of the cost of a sufficiently sized model and the relatively low speeds of common models. Brushless DC motors are too high speed and low torque and would have required expensive and complicated gearing to reduce their output down to something we could use, with the gearing re-introducing the vibration source of power transmission. The final choice was a brushed DC motor and a PWM DC motor controller[1]. Due to the low target speed, high desired torque and preference for direct drive without gear reduction, the AmpFlow E-150[2] stood out. As a quick solution so that we could work on aspects directly related to the balancing mechanism we chose a motor controller that came assembled and complete with physical controls so that we only needed to wire in the power supply and motor instead of spending time making a control interface.

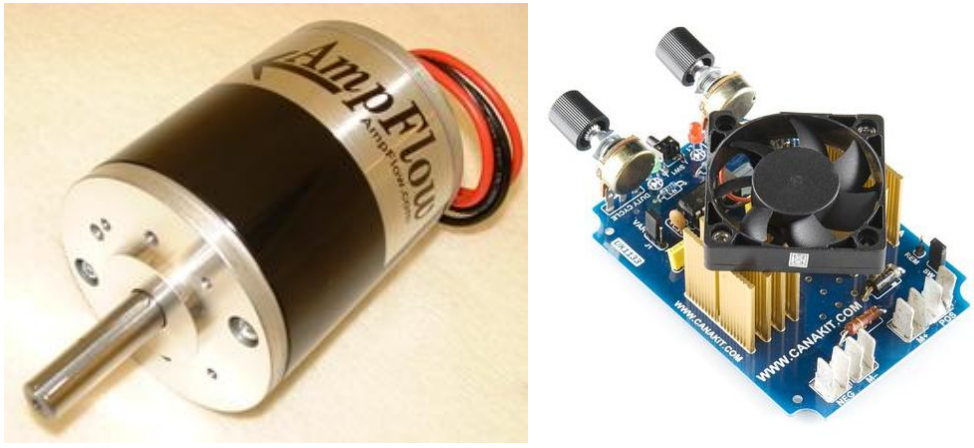

Figure 10. Motor and Controller.

III.2. Shaft Selection

With our target resonant frequency and motor selected we started working on the design for the remainder of the parts in the assembly. For a single resonant frequency we needed equal

[1] http://www.canakit.com/50a-dc-pwm-motor-speed-controller.html
[2] http://www.ampflow.com/ampflow_motors.htm

stiffness in all directions around the cantilever. In order to achieve uniform stiffness in any orientation we used a round rod for the cantilever. In order to get a rough idea of the size of our device required for our target frequency we based on theoretical model with weight estimates of the parts at the end of the cantilever as well as calculations for the stiffness of our cantilevered beam and began experimenting with different diameter and length shafts to find a reasonable sized solution. For a given target frequency there are infinite solutions for length and diameter that will result in the target resonant frequency, but we easily eliminated the extreme bounds – a very short and thin rod would have been difficult to tune accurately because tiny changes in length would make huge changes in frequency. Similarly problematic, a very large diameter rod would have required impractical length; the mechanism would be overly large. This sizing was also influenced by our goal of being able to ignore the effective mass of the shaft as negligible in comparison to the mass of the motor/disk assembly at the end. We decided that 1 meter was the longest apparatus we could comfortably accommodate and that the aim would be for a length closer to 0.5 m. From that target we chose a shaft size of 20mm to achieve our target frequency.

III.3. Design of the Motor Holder

Designing the parts to mount the motor was challenging because we wanted to maintain the alignment of the motor on the end of the shaft and have a stiff interface so that the vibrations were linear and the introduction of nonlinearity from backlash and slop was minimized. Because the motor did not have mounting points on the back end we designed a tie rod system that sandwiched the motor between a plate at the nose and an adapter plate at the back. The adapter plate had a hole to pass the motor wires through, cupped the back plate of the motor, and had a socket in the bottom that the cantilever shaft slid into and was secured by a pair of setscrews tightening onto flats on the shaft.

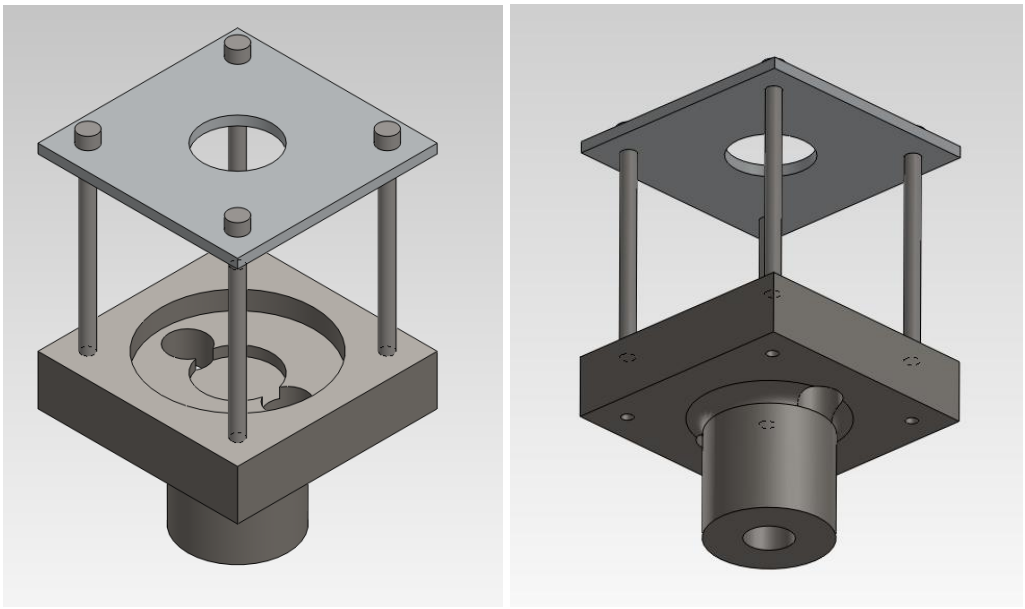

Figure 11. Design of the motor holder.

III.4. Design of the Disk

The design of the disk also had many constraints. We decided early on that the disk should be machined out of steel because the ball bearings needed for the balancing mechanism would be hardened steel and would exert large pressures on the inside of the track as the disk spun. We read that the balls had the potential to deform their raceway and we wanted to avoid that if possible (Horvath, 2008). Having selected steel as a material, the rough designs for the main disk were strongly influenced by the availability of material. Trying to fit everything we needed into the top of the disk was a squeeze. We needed a groove around the outside of the disk to contain ball bearings, we needed an inner wall to the groove so the bearings did not fall out and so that we could screw on a cover, we needed enough flat space in the middle of the disk to attach the unbalance and be able to adjust it along a groove, in order to make it lighter we wanted to remove the excess material in the disk, and then for strength we wanted to leave a hub for the motor shaft. All these factors made us look for the largest material we could find. We originally found 1”x8” steel bar and in our quick searches could not find larger stock without going to a steel plate format which was much more expensive. We were designing in metric units, so 8” bar

gave us a 200mm diameter disk with some extra material we could take off during machining so we could be sure it was fully round. With a closer approximation for the weight of the disk we could now decide the mass of the unbalance and the size of the balancing balls in order to achieve a measurable vibration displacement of the mechanism. During this sizing process it became clear that our 200mm disk was too small and we were not going to be able to adjust the unbalance as much as we wanted. We found a local steel supplier and discovered that they had 1”x10” steel plate and subsequently enlarged the design to use a 240mm diameter disk seen in Figure 12.

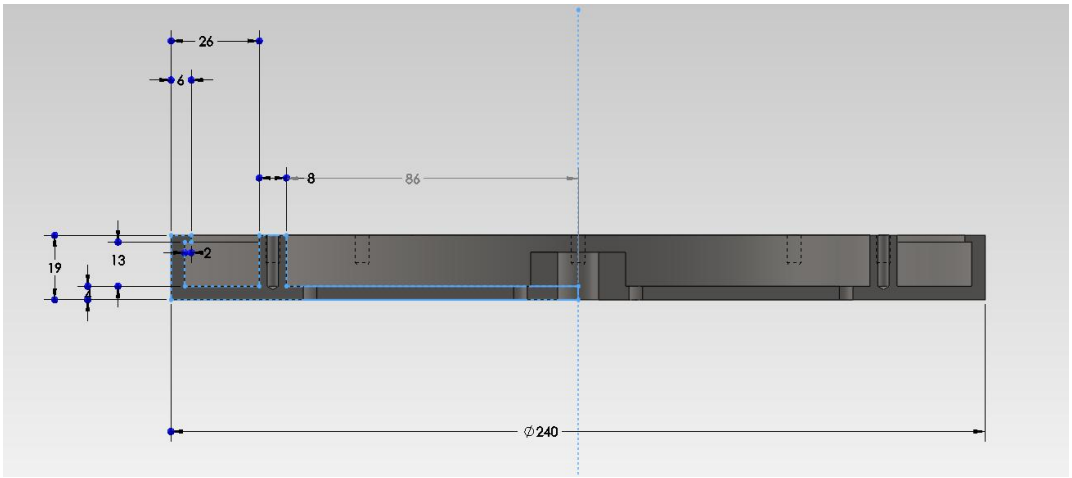

Figure 12. Design of the disk.

III.5. Design of the Clamp and Base

For the clamped end at the bottom of the cantilever we went through a few design iterations and gained some adjustment. The original idea was simply to weld the rod to a nice thick plate for the bottom end condition. While that solution provides a solid clamped fixed condition, it did not allow for any adjustment of frequency besides taking the motor assembly off, cutting off the top of the shaft and reinstalling the motor assembly. In order to more easily adjust the tuning, and lengthen the cantilever if we made it too short, we wanted to retain adjustability at this bottom clamped end. In order to maximize strength at this joint we machined

a close fitting hole in the first 1” thick block of steel that was welded to the bottom plate. We also made a two-piece shaft clamp out of another 1” thick block of steel. Our first idea was to weld half of this clamp to the bottom block (see top image, Figure 13), but we quickly decided against this plan for two reasons. The close tolerances would have made lining up the center 20mm holes very difficult and welding the piece down if it was out of alignment would likely have caused the shaft to not fit into the lower block. The points at the end of the weld would also have been very susceptible to fatigue cracking. The solution was to drill 3 slightly oversize holes in the shaft clamp and drill and tap a similar pattern of holes in the bottom block. This allows us to tighten the shaft collar around the shaft, and then bolt the shaft collar down to the base, and the slightly oversize bolt holes allow the center 20mm hole to line up accurately (see bottom image, Figure 13).

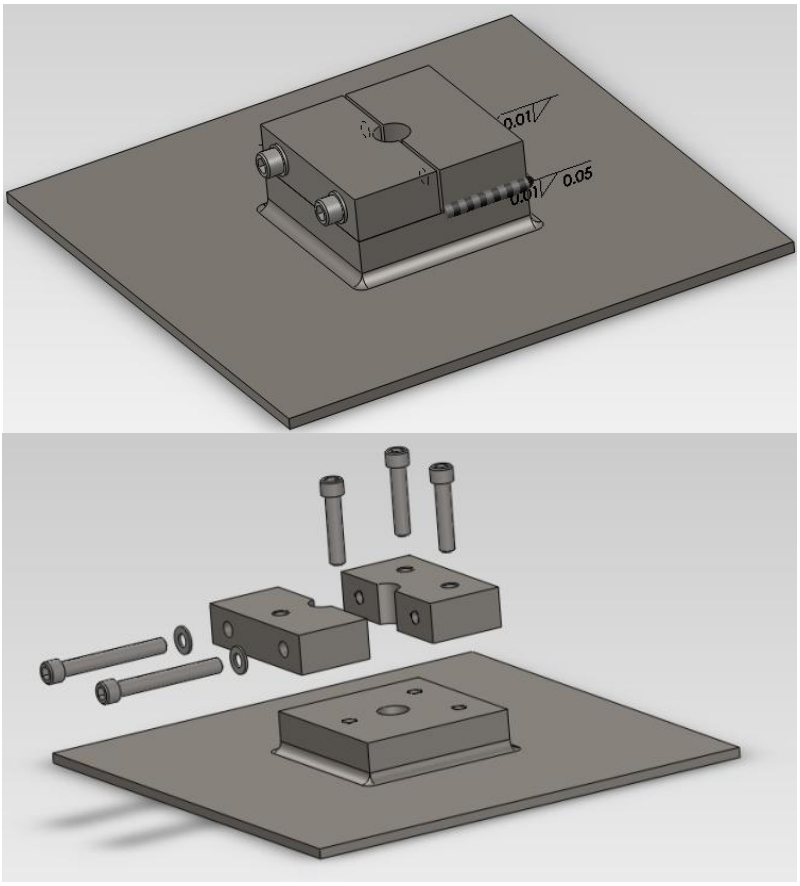

Figure 13: Designs of the Base Clamp

III.6. Manufacturing the Parts

The original design of the parts was done using metric units for simplicity in calculating the resonant frequencies and to standardize to one system rather than calculating for resonant frequency using metric units but machining the parts in SAE. This choice was mostly trouble free throughout the part ordering and design phase up until machining. The motor we chose had a metric sized output shaft and keyway, and metric sized ball bearings and shaft for the cantilever were easy to find. The problems began when we started specifying tooling to use during manufacturing. The Washburn Shops at WPI only stock SAE sized mill bits, drill bits, and taps. The mill bits were not an issue, because the CAM software could easily compute and compensate for SAE bits and a metric sized part, but the drills and taps were problematic. This tooling constraint caused last minute changes and eventually caused a problem.

The problem occurred with the bolt holes for holding the cover onto the disk to keep the balls inside their groove. The original specification for these holes was a 4mmx0.7 thread. The tap drill would have been 3.3mm but the shop only has inch, number and letter drills. The inch equivalent of 3.3mm would be .1299, and the closest size available was a #30 drill. For a hole that would be tapped, that is just fine. However the issue came after the holes were drilled and the tapping started. A member of the team inspected the holes, found a tap that seemed approximately correct and began working until the second hole when 'bang' the tap snapped off in the hole. Upon closer inspection, because of the unavailability of metric taps, the member chose what he thought was the SAE tap that matched the hole. The hole was obviously too big for a #6-32 thread, and obviously too small for a #10-24 thread, so he decided it must be a #8-32 thread and began to tap the holes. The problem here is that the holes were drilled with a #30 drill (0.1285 in) and the #8-32 tap hole is specified at #29 (0.136 in). Drilling out those extra 8 thousandths of an inch with the tap proved to be too much strain and the tap broke and lodged itself in the hole. After discovering this error the remaining holes were drilled out with a #29 drill, tapped, and there were no further sizing issues. We reviewed the number of bolts holding the lid onto the disk and decided to use only 4 instead of the original 8.

Another design change caused by manufacturing issues was the straight walls of the ball bearing raceway. The original design was undercut so that the balls did not rely on the lid to stay in the groove while the system was at operational speed. The top lip of the undercut would be a stronger barrier to keep the balls down in the disk. During preliminary manufacturing and design review we verified that the machine shop had cutters capable of making such an undercut, but there was a communication error and the shop did not realize we were cutting steel. Later during manufacturing we learned that their undercutting tools were not suitable for cutting steel and that

we would need to purchase our own. An undercutting tool was ordered and arrived, but we made a mistake in programming the tool path in the CAM software and the tool broke off in the work piece. With dozens of hours of machining time invested in the part and the possibility of a redesign, we did not want to use our second piece of steel and remake the disk, so we filled the tool crash area with weld and re-machined the groove to smooth the rough weld filler. At that stage we no longer had time to order a new cutter and attempt the undercut again, so we changed the design to have a straight walled groove and eliminated the undercut operation altogether.

Because of our choice to use a 250mm disk, our part was too large for the HAAS MiniMills in the shop. We were able to use the larger HAAS VM3 in the shop for machining the disk but it took longer because we could only use it during times when direct supervision was available. The VM3 is much more rigid than the MiniMills and has stronger motors to drive the moving axes in the machine. While it ultimately took longer than if we could have used a MiniMill because of supervision, the superiorities of the VM3 significantly reduced the active machining time on the part once we became comfortable with the higher feed and speed capabilities of the big machine. Due to their availability we used the smaller MiniMills for the other machined components in the system.

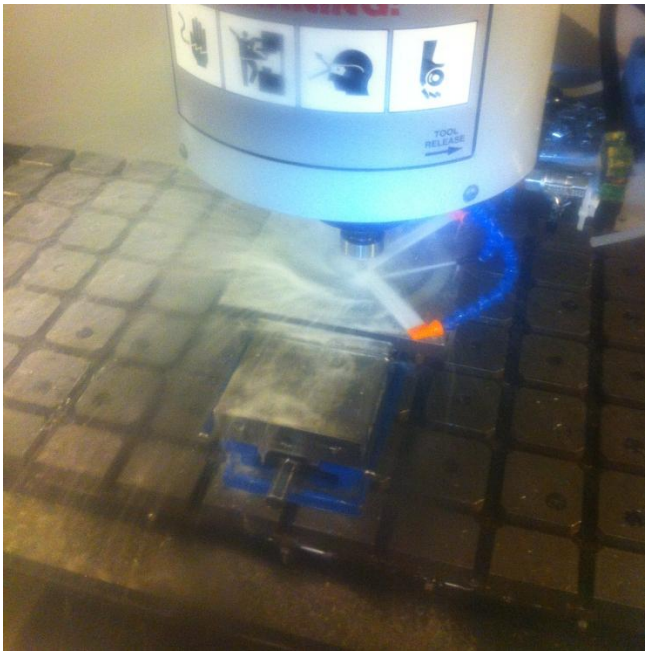

Figure 14: Machining the Disk in the HAAS VM3.

Our finished devices are shown in Figure 15. The motor is clamped on a heavy optical breadboard.

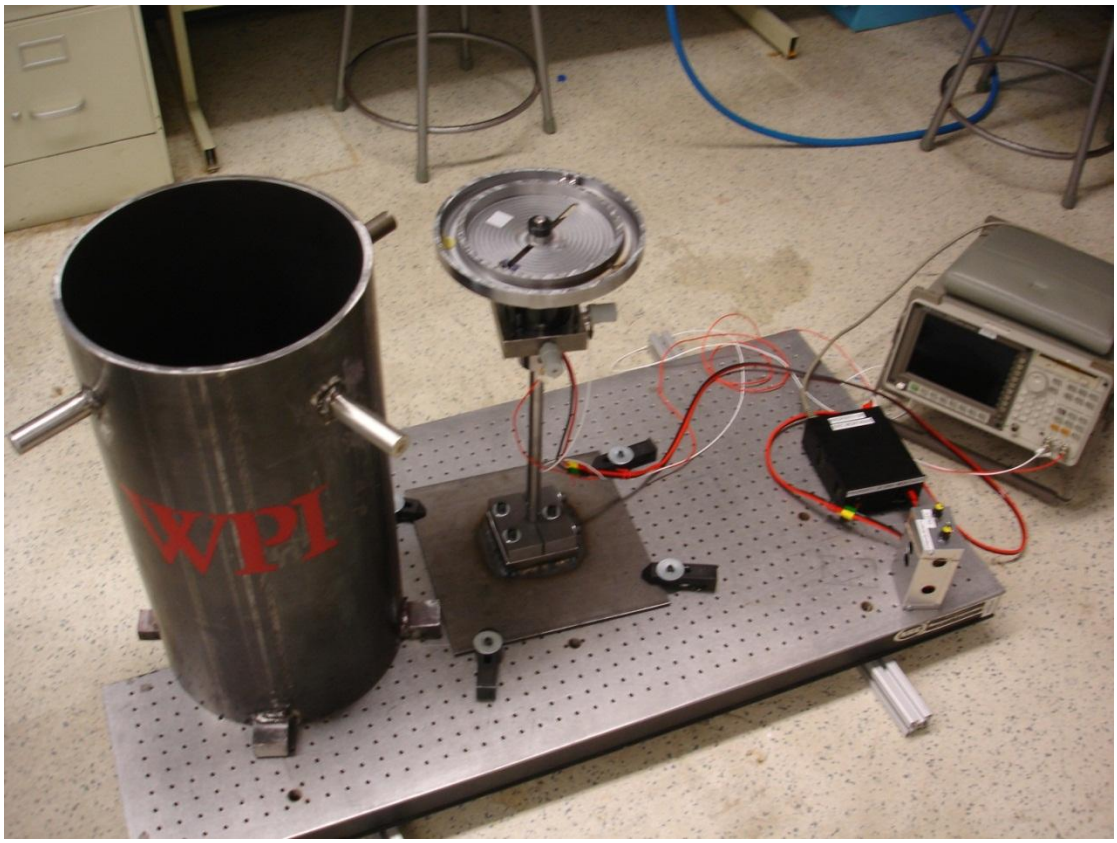

Figure 15. Our finished system with a large pipe used for protection.

IV. Experiment

IV.1. Stroboscopic system

A strobe system is needed to observe the motion of the disk as well as the balls inside the groove. By the strobe we can see by naked eye the live image of the positions of the balls in the groove, or the relative motion of the balls relative to the disk by adjusting the frequency of the laser pulse. The setup of the optic equipment, including laser source, laser modulator which is driven by a function generator, lens and mirrors, is shown in Figure 16.

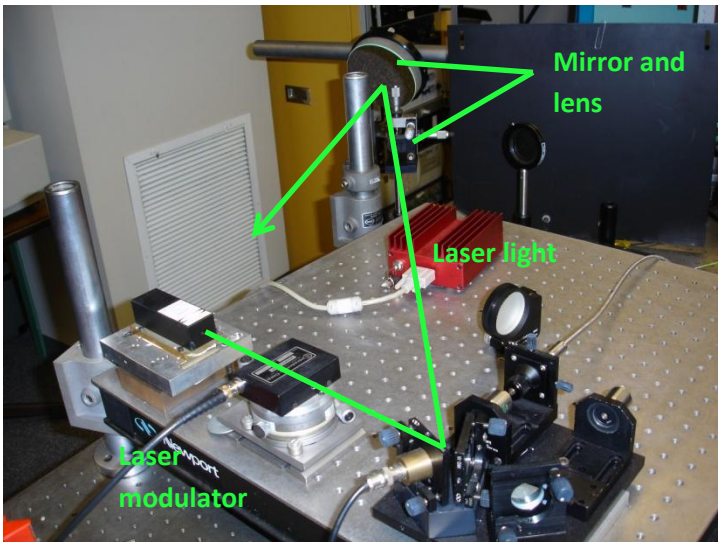

Figure 16. Setup of optical equipment for strobe.

The signal fed into the laser modulator has the form shown in Figure 17. The frequency of the pulse needs to be exactly the same as the disk rotation frequency to give a still image. Higher duty cycle gives brighter but more blurry image and via versa.

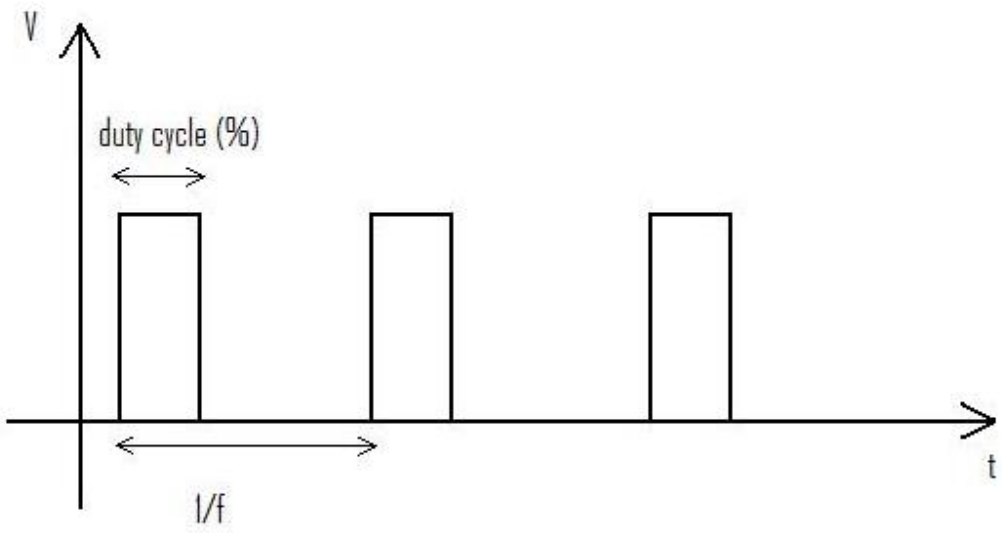

Figure 17. Signal form that drives the laser.

The disk is run under the stroboscopic illumination. When we know that the balls are settled, we use a high speed camera mounted on top of the disk to take pictures, as shown in Figure 18.

Figure 18. The disk under strobe light and camera.

IV.2.Data Acquisition system

We first plan to use a dual axis MEMS accelerometer with a DAQ assistant in LabVIEW to record the x and y motion of the disk. However, its noise level is too high so we switch to a pair of piezoelectric accelerometers and an HP 35670A Dynamic Signal Analyzer to record the signal. To measure the resonant frequency of our system as well as the live rotation speed of the motor, the signal in time domain is transformed to frequency domain using Fast Fourier Transform (FFT).

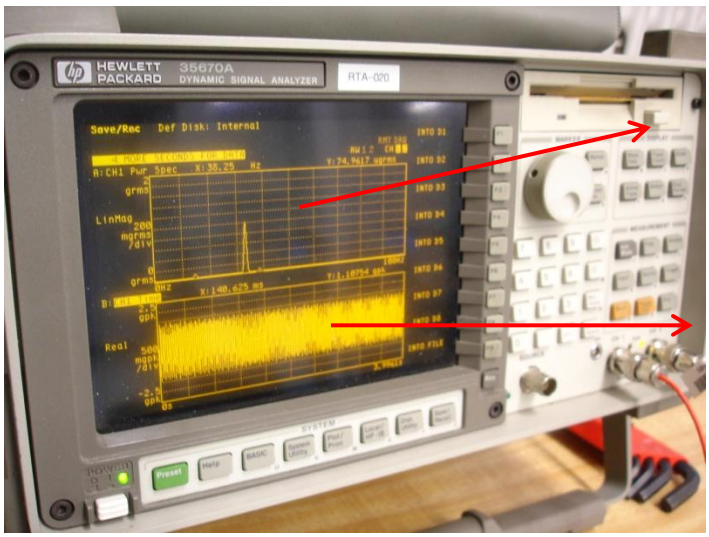

Figure 19. Display of HP 35670A.

Our setup in frequency domain is 100Hz in frequency span with 400 lines. Thus the resolution in frequency domain is 0.25Hz, and the length of the record time is approximately 4s. The time interval in the time domain is about 3.9ms, so the sampling rate is 256Hz. Our plan is to run the disk within a few times of resonant frequency, which is planned to be 13.5Hz, so the Nyquist criterion for sampling frequency will always be satisfied.

The sensitivity of the accelerometers is known to be 100mV/g, so we can convert the voltage signal to acceleration and displacement signal. If the displacement amplitude is X and the acceleration amplitude is A, their relationship is:

$$X = \frac{A}{(2\pi f)^2} \tag{20}$$

where f is the rotation speed in Hz. Thus if the acceleration and the rotation speed are known, we can calculate the displacement amplitude.

IV.3. Procedure

The goal of the experimentation phase of the design project was to create a proof of concept of a self-balancing rotor as well as measure the change in unbalance affected by the balancing mechanism. Doing this required a method to observe the device while in motion and a method to measure and record the imbalance in the rotor. The experiment also required that changes to the variables of the system were recordable. One experiment was performed to observe the motion of the ball bearings as they moved into position in the race of the rotor, and another experiment was performed to observe the deflection of the shaft during operation.

To observe the device in motion, the device was moved to one of Worcester Polytechnic Institute's Center for Holographic Studies and Laser micro-mechTronics (CHSLT) laboratories. The device was clamped rigidly between two optical breadboards. The lab's stroboscopic laser was pointed at the top of the rotor so that its movement could be seen during operation. The motor was then activated and the system was brought up to full speed, about 40 Hz. Because the device did not have a trigger signal for this experiment, the frequency of the stroboscope had to be adjusted manually. The HP 35670A signal analyzer was able to provide the approximate frequency of the system in the form of a peak created by performing a fast Fourier transform (FFT) of the signal provided from one of the piezoelectric accelerometers. This approximate frequency was entered into the stroboscope's controls and then fine-tuned to match the actual frequency of system. A Nikon D700 and a Sony DSC P100 were used to record the position of the balls when the system was in steady-state. The time elapsed before the system reached

steady-state was also recorded. This process was repeated with different natural frequencies, which was adjusted by lengthening the distance between the shaft clamp and the rotor. The equation that governs the change in natural frequency is equation (4). The experiment was performed with a number of ball bearings ranging from two to eight and two different size mass unbalances: 17.6g and 82g. The radial distances of these unbalances could be varied from 27-77mm. The effects of increasing the acceleration of the motor as it passed through the natural frequency of the system were observed. The results of these experiments are available in Part V.2 page 42.

The purpose of the second experiment was to measure the deflection of the shaft and to observe the effects of damping on the elapsed time before the system reaches steady-state. Due to oil containment issues, the experiment could not be carried out in the CHSLT lab and the device was moved into WPI's engineering experimentation laboratory. The device was clamped to a single optical breadboard and the shaft length was changed to yield a natural frequency of approximately 12 Hz. For this experiment, a tachometer was created using an optical sensor that generates an infrared light beam and records the reflection which output a trigger signal once per revolution when a piece of retro-reflective tape, stuck to the top of the rotor face, passed the sensor. The addition of a tachometer allowed more accurate measurement of the system's frequency and allowed the HP 35670A dynamic signal analyzer to display a two-channel orbit plot of the acceleration of the rotor in its horizontal plane.

To perform the experiment, damping fluid was added to the race of the rotor (except during control runs) as well as two to eight balls. The motor was then switched on and the system was brought up to full operating speed, approximately 40 Hz. The acceleration and angular position data was saved to a floppy disk and exported to MATLAB. The position of the

ball bearings in the race was recorded using a Sony DSC P100. The effect of two different lubrication agents, 80W-90 gear oil and lithium grease, were observed. In between runs, fluid was added to replace what was lost through the joint between the rotor and the clear acrylic lid. In some cases in the experiment, the system could not reach steady-state or could not achieve an optimum balance state, where the accelerations were either the same as the control (unbalanced) state or were not significantly lower than the control state. In these cases, the effect that induced vibrations, caused by slowing the rotor until the system reached its natural frequency, had on achieving a steady-state balance condition were observed.

V. Result

V.1. Verification with theoretical model

First, while the motor is off and the disk is not running, the disk is hit several times and its decaying response is recorded to measure the damping ratio due to internal friction in the shaft. A decaying function is fit to the decreasing peaks:

$$x = Ae^{-\zeta\omega t} \tag{21}$$

Since the disk is vibrating freely, it vibrates at its natural frequency. Thus, the damping ratio can be extracted from equation (21). The decaying vibration and the fitted curve are shown in Figure 20.

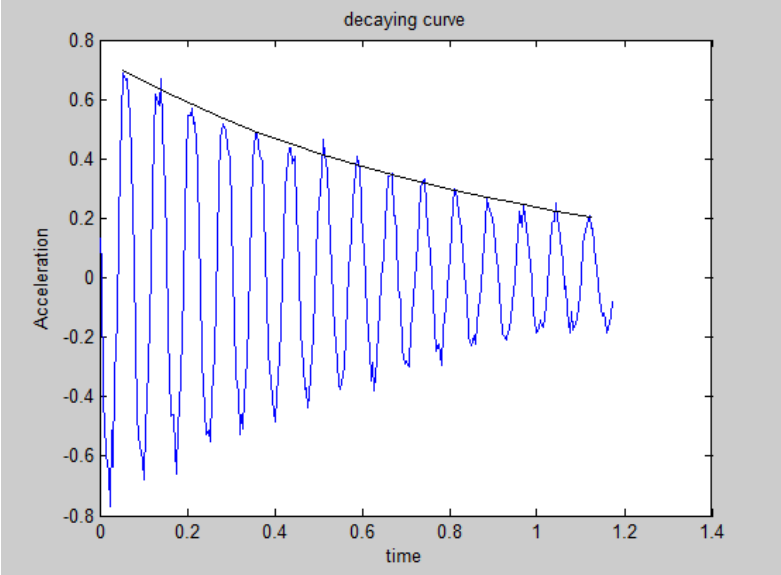

Figure 20. Decaying vibration of the disk due to internal friction in the shaft.

The damping ratios obtained from several tests are averaged. The result is summarized in Table 5.

Table 5. Result of damping ratio test.

	Damping ratio
Test 1	1.35%
Test 2	0.91%
Test 3	1.22%
Test 4	0.99%
Average damping ratio	**1.12%**

It shows that our initial estimation (0.5% to 5%, Figures 5, 6, 7) when we were designing this device is close.

Next, we verify that the actual first natural frequency of the system matches with our theoretical model. For our desired setup, we measure the distance from the fixture to the center of gravity of the mass at the top as the effective length, as shown in Figure 21. The center of gravity of the mass at the top is found from the CAD model, which is about 124mm from the bottom of the motor holder. The length of the shaft is about 340mm. Thus the effective length is 464mm (close to our desired value of 500mm).

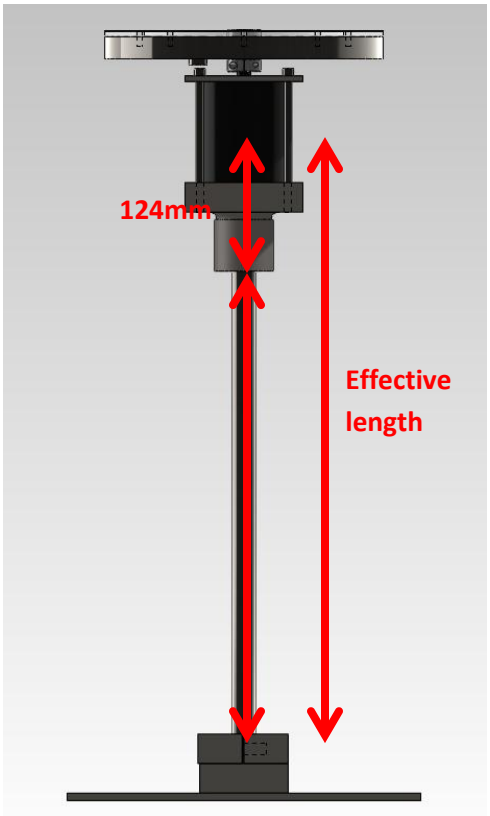

Figure 21. Center of mass at the top of the shaft.

Also, we weigh our parts to obtain their real masses. The balls and the unbalance were weighed using a micro scale in CHSLT lab, while heavier parts were weighed using a coarser scale. The real values are checked with those used in the CAD/theoretical model in Table 6 (please note that the values in CAD/theoretical model also change a little from the initial design).

Table 6. Real mass vs. mass used in CAD/theoretical model.

	Real values	**Values in CAD/theoretical model**
Mass on top of the shaft (including motor holder, motor, disk, fasteners, etc.)	6.4kg	6.8kg
Mass of the shaft	0.9kg	1.2kg
Mass of each ball	7.05g	7.10g
Mass of the unbalance	82.5g (or 17.6g)	100g

Thus, from equation (4), the first natural frequency for this system is checked again with real values:

$$f_n = \frac{1}{2\pi}\sqrt{\frac{3EI}{L^3(M + 0.23m_{shaft})}} \approx 13.57Hz$$

It matches surprisingly with the natural frequency measured by the dynamic signal analyzer, which is about 13.5Hz. In fact, we can increase the resolution of the analyzer to obtain a more accurate result of the natural frequency, but it is not necessary because we will operate very far from this frequency, not in the vicinity of it.

V.2. Tests of the self-balancing effect

In this part, the eccentric disk is run in different conditions such as amount of unbalance, number of balls, damping in the groove, and speed.

First, the length of the shaft is adjusted so that the resonant frequency is lower. We record a resonant frequency of 7.75Hz in this case. The unbalance used is just a bolt with a nut at the farthest distance in the slot. Hence the unbalance mass is 17.6g at about 77mm from the disk's center, which is shown in Figure 22.

Figure 22. 17.6g unbalance mass radius≈77mm

The number of balls added needs to satisfy equation (12). For the case of two balls:

$$2m_{ball}R_{ball} \approx 1.523\ kg * mm \quad (22)$$

$$m_{unbal}d_{unbal} \approx 1.355\ kg * mm$$

Thus, assuming that the disk alone is well balanced (which may not be the case), two or more balls should be enough. In the end, the numbers of balls tested are 2, 3 and 4. Table 7 summarized the steady-state amplitude of the vibration of the disk at different rotation speed.

Table 7. Summary of the first set of tests.

Natural frequency	Unbalance	# of Balls	Rotation speed (Hz)	Mean Amplitude (mm)	Normalized Amplitude
7.75Hz	17.6gx77mm	0	25.25	0.765	1
7.75Hz	17.6gx77mm	2	15	0.526	0.687581699
7.75Hz	17.6gx77mm	2	25.25	0.826	1.079738562
7.75Hz	17.6gx77mm	3	16.5	2.485	3.248366013
7.75Hz	17.6gx77mm	3	31.5	0.404	0.528104575
7.75Hz	17.6gx77mm	4	11.25	5.202	6.8
7.75Hz	17.6gx77mm	4	25.25	0.0917	0.119869281

The normalized amplitude is the actual amplitude divided by the amplitude without the balls, so normalized amplitude smaller than 1 is desired. Table 7 shows three times in which the steady-state amplitude is worsened. The first case is 2 balls at 25.25Hz, in which the normalized amplitude is almost 1. Theoretically as the rotation speed increases further from the resonant speed, the amplitude should be reduced, so 25.25Hz should give better result than 15Hz. However, in this case we did not increase to 25.25Hz from 15Hz. Instead, from 15Hz we turned the motor off until the disk stopped, and then we increased the speed again to 25.25Hz. Thus the balls were settled in different positions which are not as ideal as the previous positions. Later tests also confirm that the balls can settle very differently if the disk is stopped and run again.

For the case of 3 and 4 balls, the disk was not stopped and it is shown that operating further from resonant frequency can give significantly better result. Although it can still work as in the case of 2 balls at 15Hz, running at less than twice the resonant speed is not recommended.

A problem in this sequence of tests is that, without any damping in the groove, it may take very long time (2-3 minutes or more) for the balls to settle in stable positions. The reason is that the balls can overshoot their stable positions many times. With the strobe light, we can tell that while looking for their stable positions, the balls move in groove at resonant frequency of the system and make the vibration much more severe. Thus, the next sequence of tests, we always add damping fluid in the groove and the balls can find their stable positions almost immediately after the resonance is passed.

In the next sequence of test, we change the length of the shaft so that the resonant frequency is back to our designed value of 13.5Hz. We also add some drops of damping fluid to the groove (Figure 24) and speed up the motor from rest to at least 2.5 times the resonant frequency. Moreover, in addition to 17.6gx77mm unbalance, heavier unbalance of 82g, as shown in Figure 23, is also tested.

Figure 23. 82g unbalance mass at radius≈27mm. It can be moved to radius of 72mm.

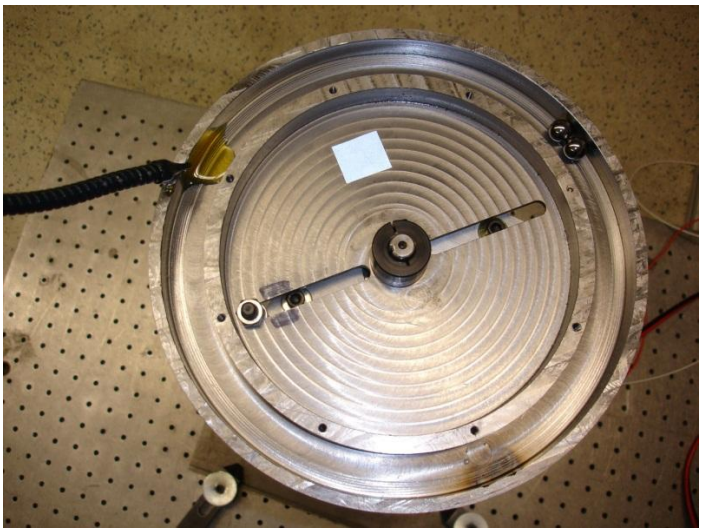

Figure 24. Amount of damping fluid added.

Equation (12) is checked:

$$m_{ball}R_{ball} \approx 0.762\ kg * mm$$

$$m_{unbal}d_{unbal1} = 82g * 27mm \approx 2.214kg * mm \quad (23)$$

$$m_{unbal}d_{unbal2} = 82g * 72mm \approx 5.904kg * mm$$

Thus, it is shown that for 82gx27mm unbalance, we need at least 4 balls, and for 82gx72mm unbalance, we need at least 8 balls.

Table 8. Summary of second set of tests.

Natural frequency	Unbalance	# of Balls	Rotation speed (Hz)	Mean Amplitude (mm)	Normalized Amplitude
13.75	17.6gx77mm	0	35.25	1.223	1
13.75	17.6gx77mm	2	32	1.367	1.117743254
13.75	17.6gx77mm	2	43	1.51	1.234668847
13.75	17.6gx77mm	4	43.25	0.611	0.499591169
13.75	82gx27mm	0	38.25	2.875	1
13.75	82gx27mm	4	43.25	0.9596	0.333773913
13.75	82gx72mm	0	42.75	7.159	1
13.75	82gx72mm	8	43.25	0.4615	0.064464311

Table 8 summarizes the steady-state vibration amplitudes for this sequence of tests. Except for two cases with 2 balls in which the vibration is made slightly worse, other tests successfully reduce the vibration. It is also shown that with the damping fluid in the groove, the balls can find their stable positions almost immediately or within only a few seconds after the resonance is passed. The unsuccessful case is again due to the balls did not settle in ideal positions. Ideal positions of the balls should yield:

$$m_{ball}R_{ball}\sum cos\phi_i \approx -M_{unbal}d_{unbal} \quad (24)$$

where ϕ_i is the angle of the *i*th ball with respect to the unbalance.

In Figure 25 we summarize the normalized steady-state vibration amplitudes for the tests at 2.5 times the resonant frequency or above, since we think this domain give the best results.

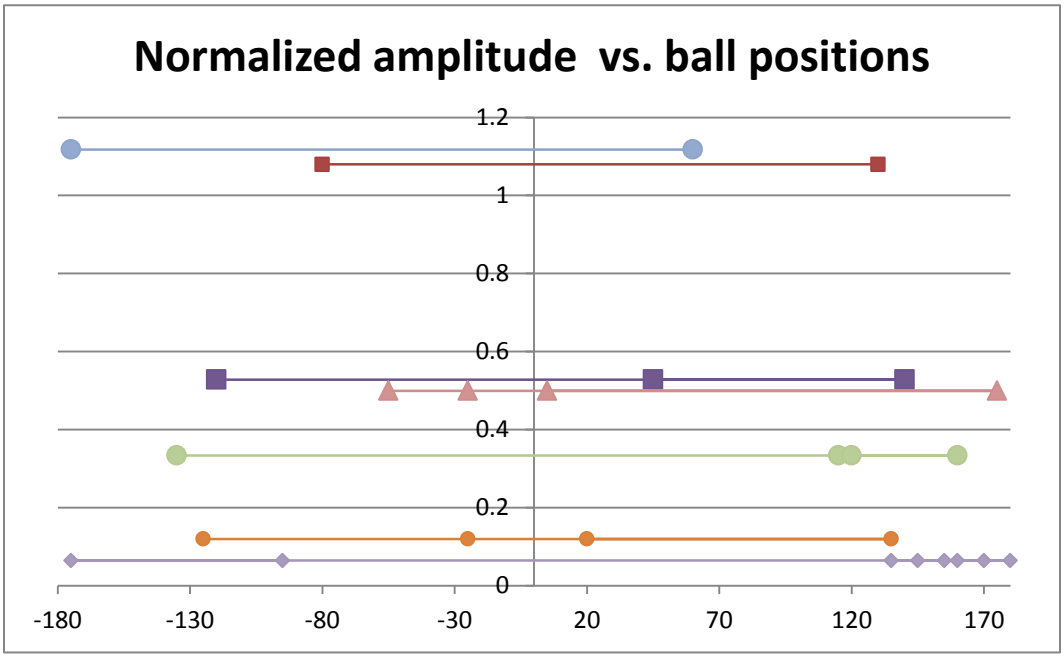

Figure 25. Normalized steady-state amplitude for tests at 2.5 times resonant frequency or above.

As mentioned earlier, each time the disk is stopped and then run again, the balls can find very different stable positions and not all of them are ideal (satisfying equation (24)). Figure 26 shows different settled positions for 2, 4 and 8 balls. Also as shown earlier, an odd number of balls can also work, and the settled positions for 3 balls are also shown in Figure 26.

Figure 26. Different settled positions of the balls.

For demonstration, we have also done additional tests with Orbit display on the dynamic signal analyzer. Therefore, instead of time response of only one channel, now the signals from both the accelerometers over time can be plotted on x and y axis. To do this, a tachometer is set up in the system. This tachometer will send a signal to the analyzer whenever a reflective paper passes by its head, which marks one revolution. The test setup is shown in Figure 27, which shows that we use 17.6gx77mm for unbalance with 2-ball balancer. The motor is run at full speed (2600rpm or 43.3Hz).

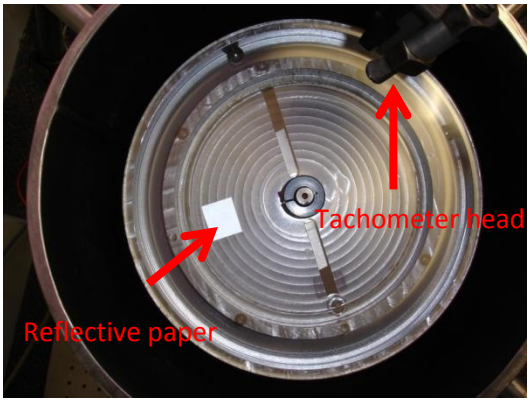

Figure 27. Setup for tachometer.

The motor is stopped and run several times and the orbit is recorded for each time. The results, which are loops of x and y acceleration, are shown in Figure 28.

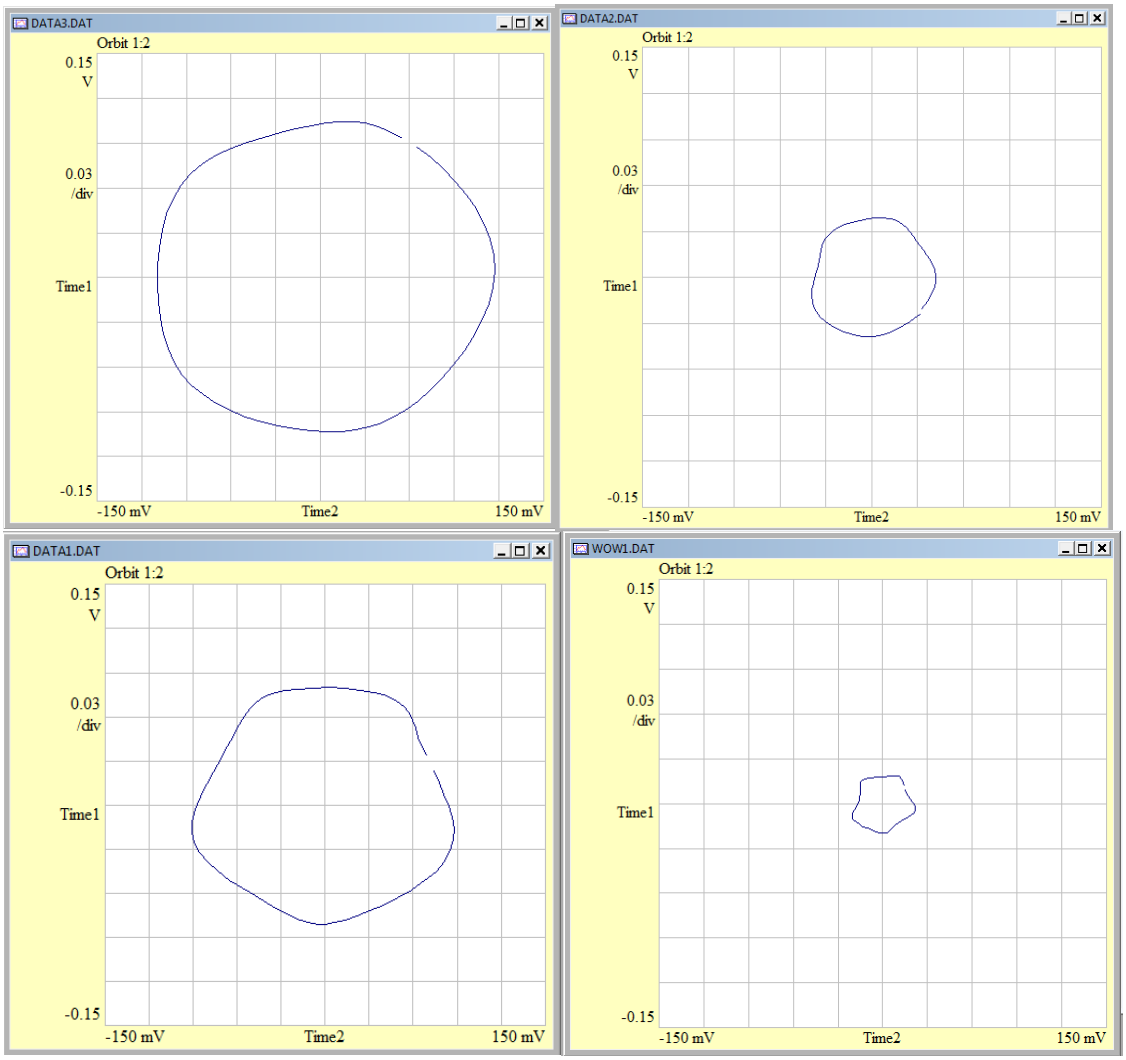

Figure 28. Orbits of 4 tests. The upper left orbit is without the balls, the other 3 are with 2 balls.

Although plots in Figure 28 are acceleration plots, according to equation (20) we can also compare them as amplitude since all the tests are at the same rotation speed. This test once again confirms that the balls can settle in different positions when the motor is stopped and run again, so the amount of the balancing effect varies. In this test sequence, we still encounter some cases that the ball balancer does not reduce the size of the loop of no ball balancer (not shown in Figure 28).

VI. Conclusions

The self-balancing effect using ball balancers has been achieved, but not consistently. Through our tests we observe that the results are more consistent if the motor is speed up to higher speed, preferably 2.5 times the natural frequency or above. We also identify three main problems in real application of this device. First, the severe vibration when the resonant speed is passed should be reduced. A clamping mechanism that can change the resonant frequency of the system instantly is a possible solution. Second, the balls need to find their stable positions as fast as possible. We have shown that adding damping fluid can solve this problem. Third, the stable positions of the balls are often not ideal positions. This problem can be due to over-damping in the groove. Imperfection in manufacturing can cause unpredictable vibration and worsen the above problems.

VII. Recommendation

VII.1. Design Recommendations

Through the course of designing and testing the self-balancing rotor, there are some recommendations to improve the design of the testing device, to improve the experimentation, to optimize the design for use in industrial applications. During the experimentation phase, the team realized there were some aspects of the design that could improve experimental results or ease the testing process. First, a groove should be added to the outer wall of the race. This feature was present in the original design of the rotor and was intended to be machined into the race. However, the t-slot cutter ordered to perform this operation was destroyed during the machining process. In the interest of time and money, it was decided that groove would not be machined into the rotor as it was not injurious to the goal of demonstrating the proof of concept of a self-balancing rotor. When testing, it became apparent that the groove would have helped control the oil in the race and prevent it from being lost through the gap between the bottom of the lid and the top of the rotor. In between test runs, the lid of the rotor had to be removed to add more oil and change the number of balls in the race. This process was tedious and could have been improved upon through the use of access holes in the lid or another novel approach.

Another improvement would be the use of a stroboscope during all the tests. Because of the lack of oil containment, the testing device could not be used in the CHSLT laboratory. The stroboscope could provide the observer with on-the-fly data on the position and movement of the balls in the race. During the second testing phase, only the final ball position could be recorded using a Sony DSC P100 which created a flash, providing the stroboscopic effect for a short instance. A major flaw of the stroboscope used in the CHSLT laboratory was that the frequency of the pulses had to be adjusted manually. Ideally, the stroboscope would be tuned using a trigger signal so that the pulses would adjust automatically.

Finally, the design can be improved by removing unwanted vibration (vibration not caused by mass unbalance). One source of vibration was the coupling between the rotor and the motor shaft; it is not a perfect fit. There is a noticeable amount of "slop," allowing the rotor to rotate slightly out of the horizontal plane. Placing Belleville washers underneath the shaft collars was one method discussed to reduce this slop. Another source of unwanted vibration came from a repair made to rotor. During the machining process, a tool crashed into the outer wall of the race. This was repaired by welding material back into the outer wall and machining the wall again. This repair was not perfect and rotor was slightly out of balance on that side, however the team was fortunate as the repair was directly in front of the applied mass unbalance, and thus caused minimal error. A large source of unwanted vibration was from the system as it passed through resonance. Passage through resonance appeared to negatively affect the ball bearings' ability to reach a position such that steady-state in the system was achieved. To minimize the effects of passing through the natural frequency, the motor was accelerated quickly until the system reached a frequency of approximately 1.25 times the natural frequency. A better method for minimizing the effects of resonance would be to change the natural frequency during operation. Before the device was started, the system would be made stiffer, by using springs for example. When the rotor had spun up to a higher frequency than the original natural frequency, the added stiffness would be removed, causing the system to pass through resonance extremely quickly.

VII.2. Experiment Recommendations

Along with the design of the testing device, there are some recommendations to be made for the experimentation of the device. The first involves the damping fluid: the fluid properties were not parameterized. If it was, the effect of viscosity on the damping of the ball bearings in

the race could be analyzed and the effects of different viscosity fluids could be predicted. This is important for optimization of the system for applications. Second, the device was tested with the rotor in the horizontal plane. This was done so that the force of gravity could be neglected in calculations. Even though in rotation machinery the force due to gravity is miniscule compared to the forces generated by the machine, running the device in a variety of orientations would prove that the system was robust and suitable for a wider range of applications, not just those constrained to the horizontal plane. Third, it was observed that providing an impulse to the system while in operation would cause the balls to move, often to a more balanced position. The exact mechanism for this was not examined. Creating a repeatable impulse generator would allow this effect to be examined more closely, possibly leading to more reliable and satisfactory results. Fourth, a circular protractor should have been added underneath the lid to allow easier measurement of the balls' angular positions during testing. Finally, in the experiment the rotor was only spun in the counter-clockwise direction. Since the balls do not fall into place symmetrically, the effect of rotating the rotor in the opposite direction should also be observed.

VII.3. Recommendations for Applications

The purpose of this project was to research self-balancing in rotating machinery and to create a proof of concept from the principles learned. As such, the device created was for testing purposes only. However, the concept of a rotor with ball bearing balancers is readily applicable to industry. It is best applied to rotating machinery where the position and amount of mass unbalance is unknown or is not constant. One example is a centrifuge, such as those used in the medical industry to isolate suspensions. The centrifuge is loaded by the user and the mass of the samples can differ. Typically, balancing is a task left to the user, who must load the samples such that the centrifuge is correctly balanced before the device is spun by using balance tubes.

The principle of self-balancing studied here can be applied to such a machine. One recommendation to help bridge the gap between research and application would be to increase the modularity of the system so that it can be fit to other devices. Another recommendation would be to test the effect that scaling the system has on performance. The rotor used in this design was about 9.5" in diameter. To be used on larger machines, a larger rotor would be needed to accommodate a larger mass unbalances. Smaller machines would require a smaller system for packaging considerations.

Before it can be used for industrial applications, many aspects of the self-balancing rotor will have to be optimized. The goal of optimization is to reduce the time the system spends in an unbalanced state and to make the system more robust in a variety of applications. Reducing time spent outside of steady-state operation means ensuring that the ball balancers reach their correct positions as quickly and reliably as possible. One variable that affects this is the damping fluid. In testing, only a few types of lubricating fluids were tested and the differences in their effects were not closely analyzed. Also, the amount of fluid used was not optimized. Using too little fluid resulted in insufficient damping, making it difficult for the ball bearings to come to the correct position; they would move around in the race too freely. Too much fluid would have the opposite effect, and as the frequency of the system increased the balls would not have enough tangential force to counteract the damping force. Another variable that was not examined was the starting position of the balls when the test began. Does placing the balls near their balance points decrease the time elapsed until the system is balanced? Also, what effect would holding the balls until the system passed through resonance have? Both of these variables could have positive effects on the system and should be investigated.

Finally, to ensure that system can be used in a wide range of applications, the range of mass unbalance that can be compensated for should be maximized. By increasing the number of balls used in the race, this range is increased, but using many balls has deleterious effects. Since rotor only self-balances above the natural frequency, the vibration below the natural frequency increases due to the increased mass of the system. The time elapsed until the system reaches the steady-state balance condition also increases as more balls are added to the race. The best compromise between mass, sub-critical speed vibration, vibration in steady-state, and time elapsed before the balancing condition is reached should be found. This compromise may change depending on the application.

References

Dimentberg, M., “Whirling of rotating shafts-class notes”, 2010.

Blekhman, I., “Synchronization in science and technology”, ASME Press Translation, 1988.

Horvath, R., “Passive balancing of rotor systems using pendulum balancers”, Journal of Vibration and Acoustic, Vol.130, Aug. 2008.

Green K, Champneys A.R, Friswell M.I and Munoz A.M. “Investigation of a multi-ball, automatic dynamic balancing mechanism for eccentric rotors”. Phil. Trans. R. Soc. A 2008.

Chung J. and Jang I. “Dynamic response and stability analysis of an automatic ball balancer for a flexible rotor”. Journal of Sound and Vibration. 2003.

Norton R. “Machine Design: An Integrated Approach”. Fourth edition, Prentice Hall, 2011.

Hartog D. “Mechanical Vibration”. Dover Publications. 1985.

Appendix

Appendix A: MATLAB codes to calculate damping ratio.

```
%% Calculate damping
%%
% Get date from excel file
clear; clc;close all;
load('E:\old laptop\stuff\11-12-winter\Projects\Self Balancing\Measurement\damping\TRAC10');
decay=y(550:900);
[rdecay,cdecay]=size(decay);
f1=13.5;
decay_avg=mean(decay);
decay=decay-decay_avg;%shift the curve to center about x axis

dt=xi;
fs=1/dt;%sampling rate in Hz
time=[0:dt:(rdecay-1)*dt]';

figure(1)
plot(time,decay);xlabel('time');ylabel('Acceleration');title('decaying curve');
hold on;

%% find peaks
volt=decay
peaks=[0];ptime=[0];
for i=2:(rdecay-4) %check with rdecay
   if volt(i-1,1)<volt(i,1)&volt(i,1)>volt(i+1,1)&volt(i,1)>0
      peaks=[peaks; volt(i,1)];
      ptime=[ptime; time(i,1)];
   end
end
peaks(1)=[];ptime(1)=[];
%plot(ptime, peaks,'r');hold on
%% refine peak (execute this cell until rpeaks stops decreasing)
clear j
[rpeaks, cpeaks]=size(peaks);
for j=2:rpeaks-1
   [rpeaks, cpeaks]=size(peaks);
   if j<rpeaks
      if peaks(j-1)>=peaks(j)&peaks(j)<peaks(j+1)
      peaks(j)=[];
      ptime(j)=[];
      end
   end
end
%%
plot(ptime, peaks,'g'); hold on

%% calculate damping
peaks_ln=log(peaks);

p=polyfit(ptime,peaks_ln,1);
fit=exp(p(2))*exp(p(1)*ptime);
plot(ptime,fit,'black');
```

```
%damping ratio
w1=f1*2*pi;%rad/s, first mode
z1=-p(1)/w1;
```

Appendix B: Analyze steady-state signal.

```
%% Analyze signal
% 10/21/2011
%%
% Get date from excel file
clear; clc;close all;
load('E:\old laptop\stuff\11-12-winter\Projects\Self Balancing\Measurement\snapshot\long shaft\4
balls\TEST7.MAT')
[vib]=y;
[rvib,cvib]=size(vib);
accelx_g=(vib-mean(vib))/0.1; %100mV/g
%%
f=11.25;% rotation speed in Hz

%% Calibration
accelx=9.81*accelx_g; %in m/s^2
omega=2*pi*f;
dispx=-1000*accelx/omega^2; %x displacement in mm

% time series
dt=xi;
fs=1/dt;%sampling rate in Hz
time=[0:dt:(rvib-1)*dt]';

figure(1)
plot(time,dispx);axis([0 3.5 -5 5]);
xlabel('time in s');
ylabel('Displacement in mm');
title('Disk vibration');
hold on;



%% find peaks
peaks=[0];ptime=[0];
for i=2:(rvib-4) %check with rdecay
   if dispx(i-1,1)<dispx(i,1)&dispx(i,1)>dispx(i+1,1)&dispx(i,1)>0
      peaks=[peaks; dispx(i,1)];
      ptime=[ptime; time(i,1)];
   end
end
peaks(1)=[];ptime(1)=[];

%% average amplitude
xamp=[mean(peaks);mean(peaks)];
plot([time(1);time(rvib)],xamp,'black',[time(1);time(rvib)],-xamp,'black');
```

Appendix C: Mathcad calculation.

RESPONSE WITHOUT BALANCERS

Shaft: $E_{shaft} := 200GPa$ $\rho_{steel} := 7850\frac{kg}{m^3}$ $L := 0.5m$ $d_{shaft} := 20mm$

$$V_{shaft} := \pi\left(\frac{d_{shaft}}{2}\right)^2 L$$

$$m_{shaft} := \rho_{steel} \cdot V_{shaft} = 1.233kg$$

Mass: $m_{disk} := 2kg$ $m_{unbal} := 0.1kg$ $m_{holder} := 1kg$ $m_{motor} := 3.4lb = 1.542kg$

Motor: **stall torque** $T_{motor} := 430oz \cdot in \cdot g = 3.036N \cdot m$

$$Iarea_{shaft} := \frac{\pi \cdot d_{shaft}^4}{64}$$

$$M_{eff} := m_{disk} + m_{unbal} + m_{motor} + m_{holder} + 0.23m_{shaft} = 4.926kg$$

$$K_{eff} := \frac{3E_{shaft} \cdot Iarea_{shaft}}{L^3} = 37699\frac{N}{m}$$

Disk: **Moment of inertia along a diameter:** $R_{disk} := 120mm$

Total mass: shown above $I_d := \frac{1}{2}M_{eff} \cdot R_{disk}^2$

$$D := \frac{I_d}{M_{eff} \cdot L^2}$$

Dimensionless critical speed $K := \sqrt{\left(6 - \frac{2}{D}\right) + \sqrt{\left(6 - \frac{2}{D}\right)^2 + \frac{12}{D}}} = 1.76$

Critical speed: $f_{gyro} := \frac{1}{2\pi} \cdot K \cdot \sqrt{\frac{E_{shaft} \cdot Iarea_{shaft}}{M_{eff} \cdot L^3}} = 14.152Hz$

Natural frequency $f_n := \frac{1}{2 \cdot \pi} \cdot \sqrt{\frac{K_{eff}}{M_{eff}}} = 13.923Hz$ $rpm := \frac{1}{60} \cdot \frac{1}{s}$

$f_n = 835.406rpm$

Mass eccentricity $d_{unbal} := 50mm$

$$e_G := \frac{m_{unbal} \cdot d_{unbal}}{M_{eff}} = 1.015mm$$

Parameter

rotational speed: $f := 0, 0.1\,Hz .. 25\,Hz$

stiffness in x and y K_{eff}

critical damping $c_c := 2\sqrt{K_{eff} \cdot M_{eff}} = 861.856\,\frac{N \cdot s}{m}$

damping in x and y $c_d(p_{cd}) := c_c \cdot p_{cd}$ ignore internal damping

Steady-state response amplitude of the geometric center C of the disk, assuming forward whirl, without balancers

$$Z_0(f, p_{cd}) := \frac{M_{eff} \cdot e_G \cdot (2\pi f)^2}{K_{eff} - M_{eff} \cdot (2\pi f)^2 + i \cdot (2\pi f) \cdot c_d(p_{cd})}$$

Response Amplitude

$$A_C(f, p_{cd}) := |Z_0(f, p_{cd})|$$

Phase angle

$$\varphi(f, p_{cd}) := \frac{-180}{\pi} \operatorname{atan2}(\operatorname{Re}(Z_0(f, p_{cd})), \operatorname{Im}(Z_0(f, p_{cd})))$$ degree

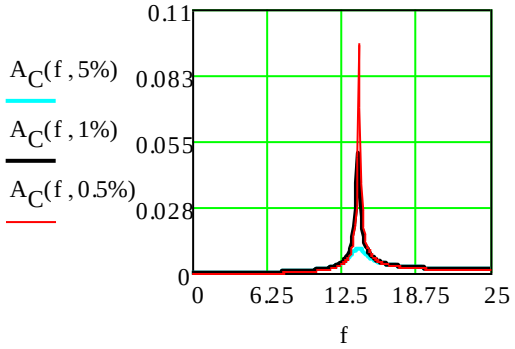

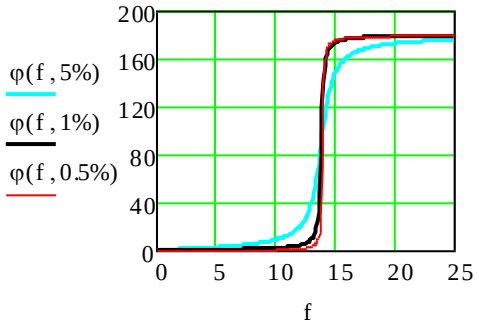

At resonance $A_C(f_n, 1\%) = 50.753\,mm$ $\varphi(f_n, 1\%) = 90$

Frequency at asymptotic amplitude $f_a := 1.5 f_n = 1253\,rpm$

Asymptotic Amplitude

$A_{Casymp5} := A_C(f_a, 5\%) = 1.814\,mm$

$A_{Casymp1} := A_C(f_a, 1\%) = 1.827\,mm$

$A_{Casymp0.5} := A_C(f_a, 0.5\%) = 1.827\,mm$

Asymptotic Phase

$\varphi_{asymp5} := \varphi(f_a, 5\%) = 173.157$

$\varphi_{asymp1} := \varphi(f_a, 1\%) = 178.625$

$\varphi_{asymp0.5} := \varphi(f_a, 0.5\%) = 179.312$

Static and Dynamic Analysis

$Y_{steal} := 351.57MPa$

Applied force

$P := K_{eff}\ A_C(f_a, 1\%) = 68.86N$

$M := P \cdot L$

$\sigma := \frac{M \cdot 0.5 d_{shaft}}{Iarea_{shaft}} = 43.838MPa$

$N_{static} := \frac{Y_{steal}}{\sigma} = 8.02$

Given: l = length, a = load location P = force I = Area Moment of Inertia E = Elastic Modulus

$l := 500mm$ $a := l$

$P := 69N$ $R_1 := P$ $M_1 := -P \cdot l$

$E := 200GPa$ $I := \frac{\pi}{64} \cdot (20mm)^4 = 7.854 \times 10^{-9} m^4$

$x := 0in, .002l..l$ $S(x, z) := if(x \geq z, 1, 0)$

$M(x) := M_1 \cdot S(x, 0m) + R_1 \cdot (x - 0) \cdot S(x, 0m) - P \cdot (x - a) \cdot S(x, a)$

Min/Max Bending Moment and Torque

$M_{max} := |M(0)|$ $M_{min} := -M_{max}$

$M_{max} = 34.5N \cdot m$ $M_{min} = -34.5N \cdot m$

$T_{max} := 0$ $T_{min} := 0$

Alternating and Mean Moment and Torque

$$M_a := \frac{M_{max} - M_{min}}{2} = 305.351\,in\cdot lbf \qquad M_m := \frac{M_{max} + M_{min}}{2} = 0\,lbf\cdot in$$

$$T_a := \frac{T_{max} - T_{min}}{2} = 0\,in\cdot lbf \qquad T_m := \frac{T_{max} + T_{min}}{2} = 0\,in\cdot lbf$$

$$\sigma_m := \frac{M_m \cdot 10mm}{I} = 0\,Pa$$

$$\sigma_a := \frac{M_a \cdot 10mm}{I} = 4.393 \times 10^7\,Pa$$

Material Correction Factors

$$S_{ut} := 421MPa$$

$$C_{load} := 1 \qquad C_{size} := 1.189(20)^{-.097} \qquad C_{temp} := 1 \qquad C_{reli} := .86$$

$$C_{surf} := 4.51\left(\frac{S_{ut}}{MPa}\right)^{-.265} = 0.909$$

$$S_e := C_{load}\cdot C_{size}\cdot C_{temp}\cdot C_{reli}\cdot C_{surf}\cdot 0.5 S_{ut} = 147.739MPa$$

Stress Concentration Factors

$$K_f := 1$$

Safety Factor

$$N_f := \frac{S_e \cdot S_{ut}}{\left(K_f\cdot\sigma_a\right)\cdot S_{ut} + \left(K_f\cdot\sigma_m\right)\cdot S_e} = 3.363$$

Appendix D: Parts List

- Ampflow E-150 Motor (http://www.ampflow.com/ampflow_motors.htm)
- CanaKit UK1133 50A DC Motor Speed Controller (http://www.canakit.com/50a-dc-pwm-motor-speed-controller.html)
- PowerWerx SS-30DV 30 Amp Power Supply (http://www.powerwerx.com/power-supplies/powerwerx-30-amp-desktop-switching-power-supply-powerpoles.html)
- 20mm Shaft (McMaster #6112K66)
- 20mm One Piece Shaft Collars (2 x McMaster #57445K73)
- 3mm key for motor/disk interface
- 12mm Hardened Ball Bearings (1 x Pkg of 12: McMaster #9292K49)
- 10”x1” 1018 Steel Bar – 24” Long for Making Disks and Base Shaft Clamp
- 0.25” 1018 Steel Plate – 12”x12” for Base
- 3”x3” 1018 Steel Bar – 4” Long for Motor Adapter/Mount Plate
- 0.25” Aluminum Plate – 3”x3” for Motor Top Plate
- 12” SCH 40 ERW Steel Pipe – 24” Long for Safety Shield (http://www.metalsdepot.com/products/hrsteel2.phtml?page=pipe&LimAcc=$LimAcc)
- Misc. Steel Scraps for Handles and Hold-Down Feet on the Pipe
- 3/8”-16 SHCS for Base
- #8-32 BHCS for Attaching Ball Retention Shield
- 0.1875” Acrylic Sheet – 12”x12” for Ball Retention Shield

Appendix E: Fully Assembled Apparatus

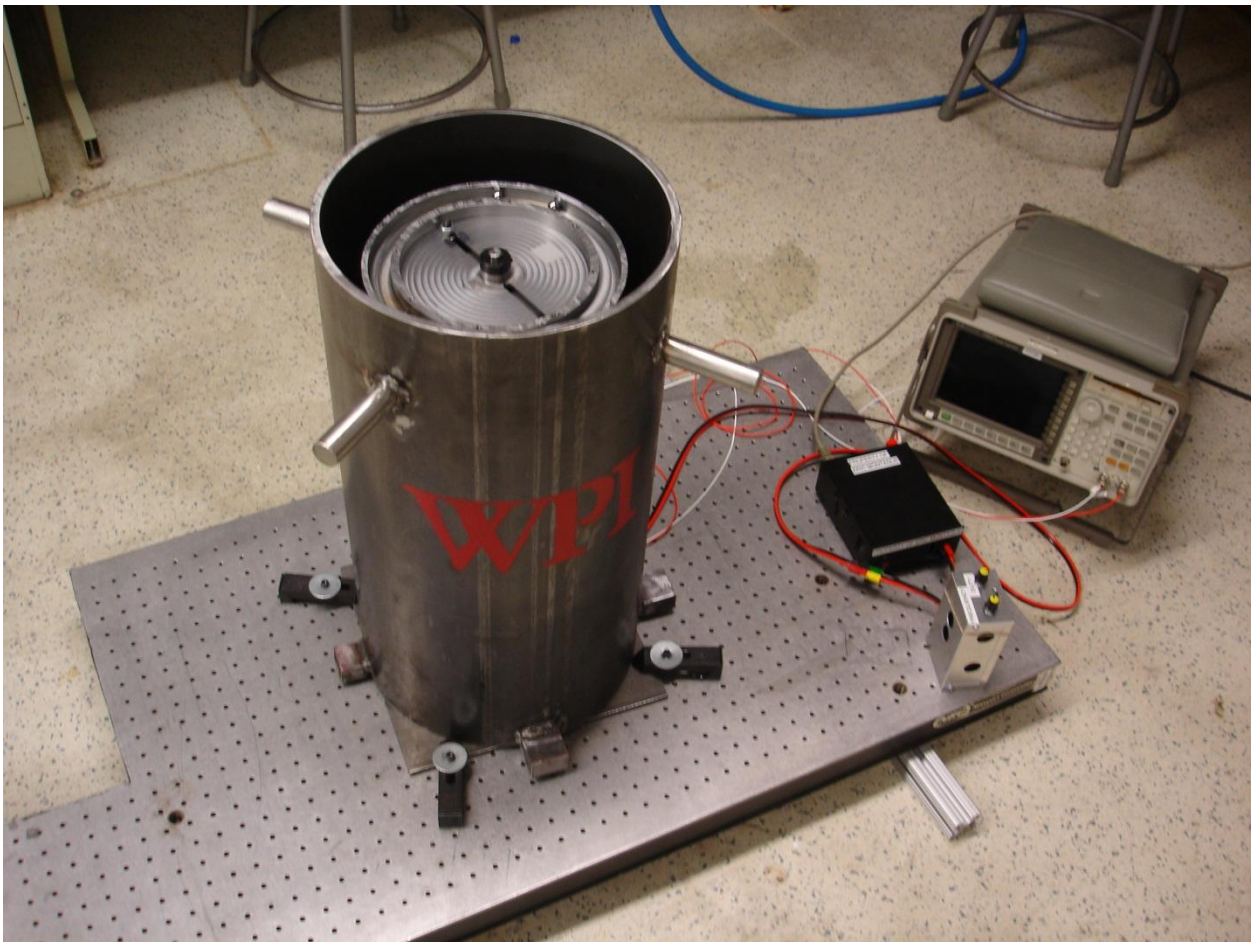

Figure 29. Assembled Testing Apparatus with Safety Shield.